Adapting FDM 3D-printing for the manufacture of microfluidic devices

Oskar Andersson

2021

Master's Thesis in

Biomedical Engineering

Supervisor: Per Augustsson

LUND
UNIVERSITY

Faculty of Engineering LTH
Department of Biomedical Engineering

Abstract

Microfluidic devices have so far not seen widespread use, even though they could potentially be cheaper, better and faster than traditional methods. A possible reason for this is the lack of a middle step between one-of-a-kind experimental devices and cheap mass produced devices. With ongoing improvements in resolution it is starting to look possible that 3D-printing will fill this role.

This thesis sought to investigate what factors limit the currently quite poor effective resolution of fused deposition modelling (FDM), an otherwise very advantageous 3D-printing technique. Specifically it looked at the effect of some of the various settings that govern the printing process, as well as the effect of nozzle diameter.

The best effective resolution (here the most the width of a channel could deviate) achieved was 15 μm, close to the optimal resolution of 12.5 μm of the 3D-printer used. The effective resolution did however vary seemingly randomly between 15 μm and 30 μm, with no correlation to any of the properties measured other than possibly the layer height. The data did however show a possible mechanism for a specific defect often seen at corners. It seems a mismatch between movement speed and the amount of material deposited may cause bumps that risk blocking small channels.

Acknowledgements

Firstly I would like to thank my supervisor Per Augustsson for providing guidance throughout this project. I would also like to thank the staff at the department of Biomedical Engineering, and Enrico Corato in particular, for providing assistance with the use of the department's equipment.

Glossary

FDM   Fused deposition modelling, a 3D-printing technique.

Print (noun)   The process of making a specific object with FDM. Can also
                       be used to refer to the object made.

Slicer   The software used to turn a 3D-model into a format that a
                       FDM 3D-printer can use to turn the 3D-model into a physical object.

Extrusion rate   The rate at which an FDM 3D-printer deposites material.

End bumps   Small bumps that form at the corners of the start and end of
                       microchannels made for this paper. See figure 22.

Contents

1 Introduction

Compared to traditional methods, microfluidic devices can have a number of advantages. They can for example have higher sensitivity [1, 2, 3] and be much faster [1], while using less sample and reagent volume [4, 5, 6, 7, 8, 9]. At the same time they can be cheaper [1] and smaller. All of this can be combined to make a centimeter-scale "chip" that can perform the same analyses as an entire lab, a so called lab-on-a-chip [10]. Such devices could be very useful in, among other things, point-of-care diagnostics [11, 12, 13, 14], cancer screening [15] and high-throughput drug testing [15].

Yet microfluidic devices have so far not seen widespread use [1, 4, 12, 8]. A common hypothesis as to why this is is a lack of a transitional step for going from making costly one of a kind devices to mass producing the same type of device [16, 17, 12].

Most microfluidic devices are currently made with soft lithography [16], photolithography [12] or micromolding [11]. Soft lithography and photolithography are useful for making experimental microfluidic devices, but require a large number of manual steps to make a single device [11]. This makes them unsuitable for mass production [11, 12].

Micromolding on the other hand is capable of making devices in rapid succession, but it is prohibitively expensive to make a new type of device [12]. This high cost is acceptable if a device is to be mass produced, but it does make micromolding less than suitable for developing new devices [11, 12, 16]. All these techniques also make microfluidic devices in very different materials, meaning that a device that works when made with one does not necessarily work when made with another [11]. They do however share one property; since they are all based on replicating some form of master mold it is quite expensive to try out a new device design.

To ease the transition from one of a kind devices to mass production, a new manufacturing method would be needed. It would ideally be capable of making microfluidic devices quickly, without a mold, from the same thermoplastics used in mass production, while also being relatively cheap. This is a quite good description of 3D-printing.

3D-printing, or additive manufacturing, is an umbrella term for a number of different techniques. What they all have in common is that they construct objects, generally layer by layer, without the need for molds or machining. Looking at the previously listed capabilities individually, there is some type of 3D-printing that can fulfill each. There are for example techniques that can make microfluidic devices quickly and without a mold, and there are techniques that can use the same thermoplastics used in mass production. But there is no technique that can fulfill all of the capabilities at once. This is however starting to change with developments in machines and materials.

This paper will focus on fused deposition modelling (FDM), a technique that essentially draws objects with molten plastic. It can already make things quickly, without a mold, from the same thermoplastics used in mass production, while also being relatively cheap. What it has had issues with so far is making microfluidic devices. While the ideal resolution of a FDM printer can be as good as $12.5\,\mu m \times 12.5\,\mu m \times 2.5\,\mu m$ in x × y × z, large amounts of defects makes the effective resolution far worse, often cited as $100\,\mu m$, and even this is dif-

ficult to achieve. This has prevented FDM from making sub-100 μm microfluidic devices, generally limiting it to the millifluidic regime.

This discrepancy between ideal and effective resolution has however not simply been left as it is. The programs used to control FDM printers can have hundreds of settings that can be adjusted to make the printing process as ideal as possible. This makes it unsurprising that it can be difficult for an inexperienced user to achieve even a 100 μm effective resolution [18, 19, 20].

To identify how to best adjust these settings it would be important to know in detail what effect they have on small features such as microfluidic channels. While previous papers have definitely managed to optimise settings, with Romanov *et al.* [21] even providing a guide for inexperienced users, the effect of settings are usually only discussed qualitatively. This paper seeks to perform a more quantitative analysis of how a selection of settings affects the quality of micro-scale channels. It will also investigate the effect of the extruder nozzle diameter, a physical parameter that has been cited as a factor limiting the quality of microfluidic devices made with FDM [18, 19, 20].

In short, this paper aims to examine how the following parameters affect the quality of microchannels made with FDM, by looking at among other things how much and how quickly the width of the channels varies:

- Nozzle temperature

- Movement speed

- Maximum allowed acceleration

- Layer height

- Cooling fan speed

- External perimeters first

- Nozzle diameter (physical parameter)

2 Background

2.1 Traditional manufacturing methods for microfluidics

2.1.1 Soft lithography

Soft lithography is currently the most common way of making microfluidic chips. A large reason for this is that the material usually used for it, PDMS, has qualities that are very useful in biomedical science. It is, among other things, biocompatible, highly flexible and transparent to a wide range of frequencies [11, 7]. Another major contributor to the popularity of soft lithography is that it is inexpensive and straightforward, due to requiring relatively little specialized equipment [11, 18, 16, 1]. It does however require one quite special piece of equipment; a master mold [11, 15, 7]. This mold is usually made using photolithography, making it quite expensive [22]. Soft lithography also involves a lot of manual steps, making it unsuitable for mass production [11, 23].

2.1.2 Photolithography

Photolithography is often used to make molds for other techniques, but it can also make microfluidic devices directly. This does however require a cleanroom environment, expensive equipment and skilled operators [11, 24, 25]. It is also not entirely free from the need for a mold; photolithography requires a photomask to make microfluidic devices [11]. It is however a very reliable method of making microfluidic devices. Photolithography also receives a lot of development thanks to its use in the manufacture of microelectronics [11].

2.1.3 Micromolding

Micromolding encompasses techniques that make micro-structures by molding a polymer on a physical mold. This includes micro-scale injection molding and hot embossing, as well as soft lithography which has been discussed previously. Both injection molding and hot embossing are more suited for mass production than soft lithography and photolithography; they are capable of making microfluidic devices in minutes or even seconds [25, 26].

Like soft lithography, injection molding and hot embossing require a master mold [27]. They can sometimes use silicon molds like those used in soft lithography, but the high pressures and temperatures present in injection and embossing machines are usually too high for silicon molds. This leaves prohibitively expensive metal molds are the only viable option [27, 11]. Such metal molds are however quite robust. One mold can be used to make hundreds or even hundreds of thousands of microfluidic devices, making the price for the mold per device potentially quite low if used extensively [27, 25].

2.2 3D-printing techniques

3D-printing, or additive manufacturing, is used to refer to manufacturing techniques that make objects by starting with nothing and adding in material where needed. This is generally done layer by layer, but how the material is added in in these layers varies between different techniques.

The use of 3D-printing in the field of microfluidics has gained significant interest in the

last decade. The reason is that the resolution of some 3D-printing techniques has started to become sufficiently good to make microfluidic channels and devices. While a wide variety of different techniques have been used for this purpose, three have received the most attention: stereolithography (SL), multi jet modelling (MJM) and fused deposition modelling (FDM).

SL makes objects from a photocurable resin that is selectively exposed in layers. As a layer is exposed it adheres to the previous one, slowly building up a complete object. The original design for SL-printers used a moving laser or focused LED light source to expose and cure the layers of resin. A more recent strategy instead uses digital light projection (DLP) to expose entire layers of resin at once [28]. Using the DLP strategy, commercial SL-printers have achieved resolutions of 15 µm (such as in the Kudo3D Micro). Printers modified specifically to make microfluidic devices have gotten even further, reaching resolutions of 7.6 µm and being capable of making channels as small as 18 µm × 20 µm [29]. Resolution is not cheap for SL-printers however; the Kudo3D Micro, at around $5000, costs 20 times as much as the cheapest SL-printers.

MJM, also known as polyjet printing, uses an inkjet head similar to that in a normal "2D-printer" to selectively deposit a low viscosity photocurable resin. This resin is then rapidly cured with UV-light. Besides the main structural material, the inkjet head can also deposit a support material. This support material is dissolved after printing, and can support the printing of complex structures [28]. Commercial machines can have resolutions of 25 µm [6], while costing atleast $6000.

FDM uses a small nozzle to deposit lines of quickly solidifying material, usually molten plastic, to form objects. While the position resolution of the nozzle can be around 10 µm, it is difficult to make features smaller than 100 µm using FDM. This is discussed further in section 2.3. The cheapest FDM-printers have prices similar to the cheapest SL-printers, at around $250, though for FDM-printers a low price does not necessarily mean worse resolution.

Since the main idea behind 3D-printing is being able to make arbitrary 3D shapes, 3D-printing techniques have the neat property of being able to make microfluidic devices with any connectors or similar already integrated. This can reduce the amount of post-processing necessary when making microfluidic devices [28]. Some of the techniques do still require some post-processing however. Objects made with SL need to be cleaned and have any channels drained of non-cured resin. Objects made with MJM meanwhile need to have any support material, such as that keeping up the ceiling of a microfluidic channel, dissolved. Microfluidic devices made with FDM on the other hand can be ready to be used the moment they are removed from the printer, though there can sometimes be some strands of material between or in connectors that need to be removed first.

If 3D-printing is to see widespread use in the field of microfluidics, it needs to be able to make devices in materials that can compete with PDMS, a biocompatible, highly transparent elastomer. While the photocurable resins used in SL and MJM tend to have issues with biocompatibility, there are resins that are specially developed for biocompatibility available for both techniques [28]. Similarly there are resins that are developed to be flexible or transparent available to both has well [16]. FDM has less issues with material selection; it can

in principle use any material that can go from liquid to solid. While most FDM printer are only designed to be able to use material in the form of thin filaments, there is a wide variety of materials available in that form. One example is the biocompatible polymer PLA, that can even be found in transparent and elastic forms.

Using these various materials, 3D-printing can be used to make microfluidic mixers, valves and pumps [14]. The more complex geometries possible with 3D-printing even allows for the use of designs that that would be at the very least impractical to make with traditional methods. Two examples of this are Baker's transformation mixers [30] and valves made from relatively rigid materials [23]. The ability of 3D-printing to make both micro- and macro-scale objects with the same machine also creates an opportunity to make simple, manually operated "world-to-chip" mechanisms [31, 14]. Such mechanism would reduce the need for bulky control systems when using microfluidic devices, which would be very useful in for example point-of-care applications.

2.3 Fused deposition modeling

FDM, as mentioned previously, can be described quite well as a method of making objects by drawing them layer by layer using a quickly solidifying material. This material is most commonly molten plastic which solidifies quickly when cooled by the ambient air. The core components of a FDM 3D-printer are a print bed, a xyz-stage and an extruder. These components will be described in more detail in section 2.4.

2.3.1 Advantages

There are a number of interesting advantages with FDM. Since the expiration of the original patent FDM has become quite popular among hobbyists. This has resulted in there being a wide array of different hobby-grade FDM 3D-printers, available for as little as $250 [28]. This popularity has also led to there being a plethora of different materials available for FDM 3D-printers, in a standardized format of thin filaments with a specific diameter.

It is also easy to use multiple materials at the same time with FDM. All that is needed is another extruder, and control electronics that can use it. It is even possible to make material gradients, by feeding multiple different materials into the same nozzle and letting them mix before depositing them.

2.3.2 Disadvantages

As advantageous as FDM may seem, it also has some serious disadvantages. The main issue is surface roughness. Since the lines of material that FDM uses to make objects are not perfect rectangles (see figure 8), surfaces made with them tend to not be perfectly smooth. This can cause increased mixing in microfluidic channels [18]. It can also affect the shape of microchannels, limiting the minimum size that is feasible to make [6].

2.4 Core components of a FDM 3D-printer

The 3D-printer used in this paper was a Creality Ender 3-Pro (seen in figure 1). It was unmodified and unused before being used in this paper.
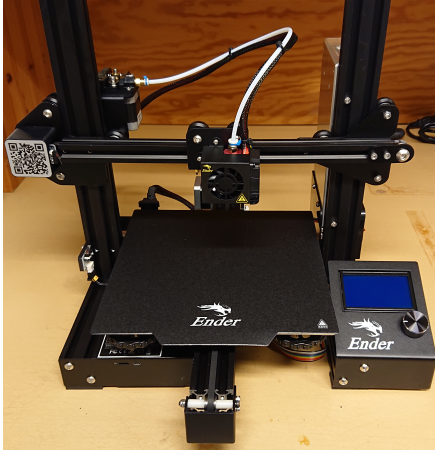
(a) Photo
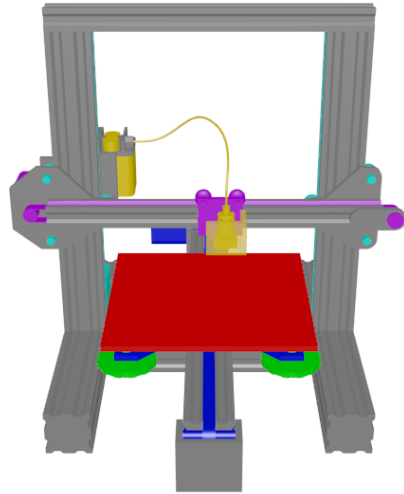
(b) 3D-model

Figure 1: The Creality Ender 3-Pro FDM 3D-printer used in this paper. a) is a photo showing the full printer, except for the top bar and filament holder. b) is an approximate 3D-model with different components marked with different colors. The marked components are the print bed (red), the calibration wheels for print bed (green), the x-stage (purple), the y-stage (blue), the z-stage (cyan) and the extruder (yellow).

2.4.1 Print bed
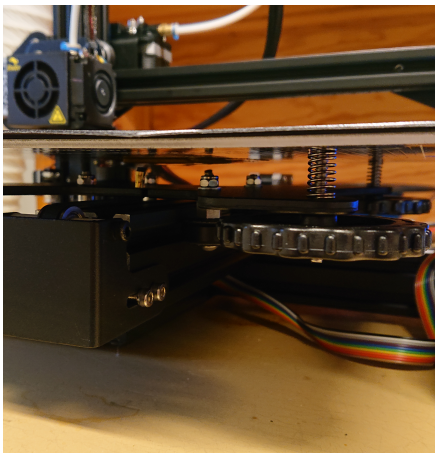
(a) Photo
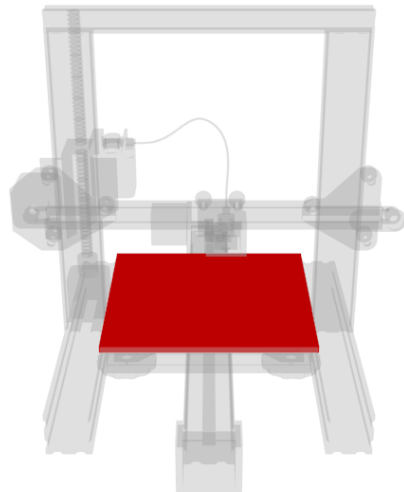
(b) 3D-model

Figure 2: The print bed of the 3D-printer. a) is a photo taken from the front right, showing the gap between the print bed and the y-stage. Two of the springs supporting the print bed can be on the right. b) is an approximate 3D-model, with the print bed shown in red.
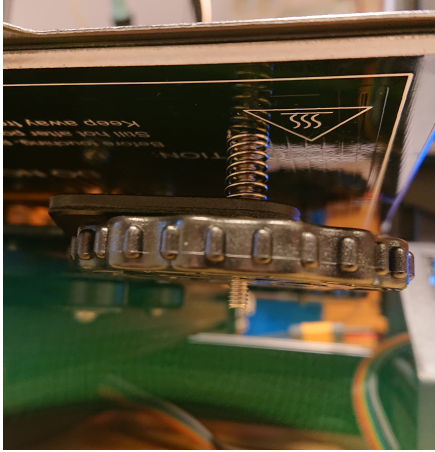
(a) Photo
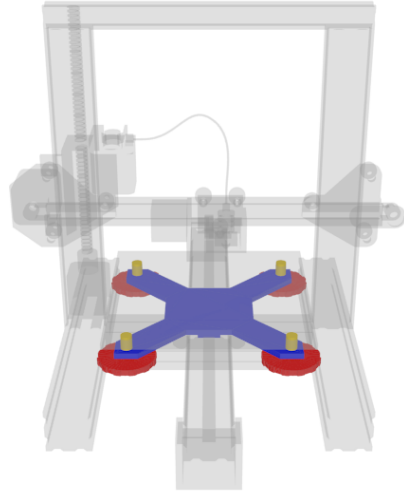
(b) 3D-model

Figure 3: The print bed calibration mechanism of the 3D-printer. a) is a photo taken from the front. It shows one of the four springs supporting the print bed. Also seen is the associated wheel and screw used when calibrating the print bed. b) is an approximate 3D-model, with the parts of the calibration system marked with different colors. The marked parts are the connection between print bed and y-stage (blue), the springs supporting the print bed (yellow) and the wheels used when calibrating the print bed (red).

The print bed, marked in figure 2b, is the surface that the first layer of an object is deposited on. Even though it only interacts with the first layer it is quite important. Since the printer cannot "see" print bed in any way, it is up to the operator to ensure that the position of the print bed relative to the xyz-stage matches what is programmed into the printer. This is often done by manually calibrating the print bed position with some form of wheel or knob (see figure 3), though some printers are capable of automatic calibration.

The print bed can also be replaced with a thin piece of transparent material, such as a microscope slide, to provide a window into microfluidic channels printed on top of it [32].

2.4.2 xy-stage
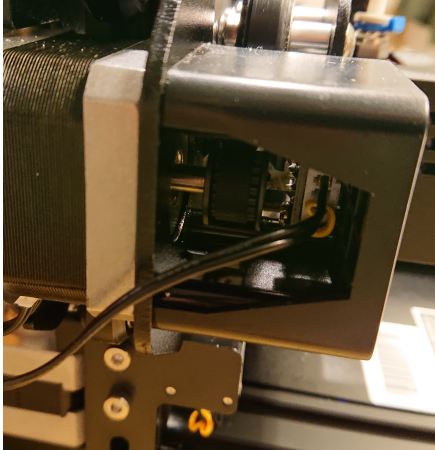
(a) Photo
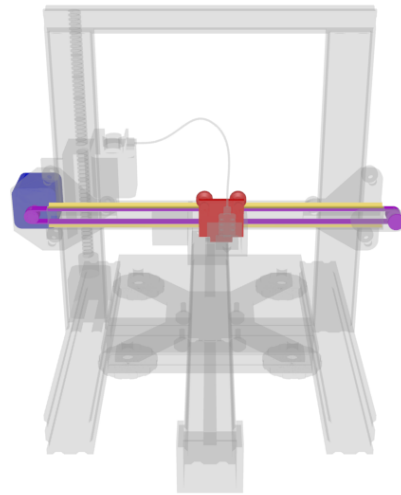
(b) 3D-model

Figure 4: The x-stage of the 3D-printer. a) is a photo taken from the left. It shows the toothed pulley and toothed belt used to move the x-stage. The pulley is directly attached to the stepper motor of the x-stage. b) is an approximate 3D-model, with the parts of the x-stage marked with different colors. The marked parts are the stepper motor (blue), the toothed belt and pulleys (purple), the moving part (red) and the track the moving part moves on (yellow). The hotend and fans of the extruder are attached to the moving part.

(a) Photo
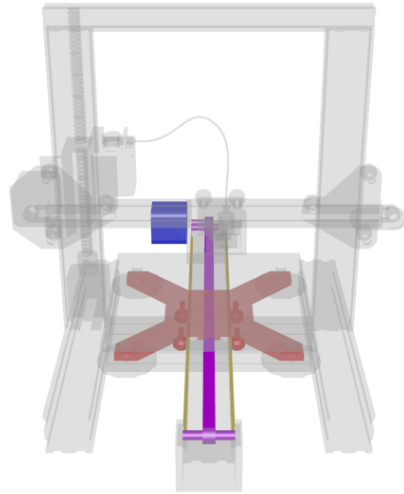
(b) 3D-model

Figure 5: The y-stage of the 3D-printer. a) is a photo of the underside of the print bed taken from the front right. It shows the wheels supporting the moving part of the y-stage, as well as the track that they move on. Note that the axles of the wheels are oriented vertically. b) is an approximate 3D-model, with the parts of the y-stage marked with different colors. The marked parts are the stepper motor (blue), the toothed belt and pulleys (purple), the moving part (red) and the track the moving part moves on (yellow). The print bed is attached to the moving part.

The xyz-stage is usually separated into a xy-stage and a z-stage, since the demands on them is quite different. The xy-stage handles all the movement of the extruder when filling in a given layer. This movement needs to be quite rapid to allow objects to be made in a reasonable amount of time. To achieve this the xy-stage usually consists of stepper motors and toothed belts moving a part along a rigid axis. The exact configuration of the xy-stage can vary significantly between different FDM-printers. In the printer used in this paper, the x-stage moved the extruder and the y-stage moved the print bed (see figures 4 to 5).

2.4.3 z-stage
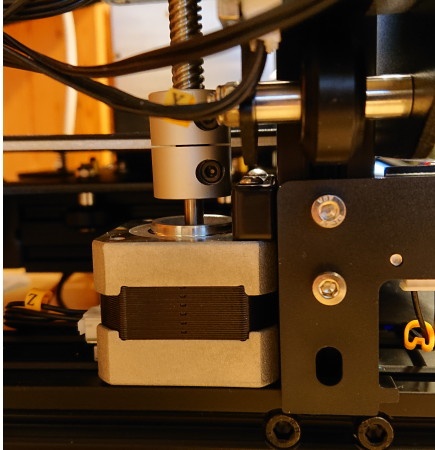
(a) Photo
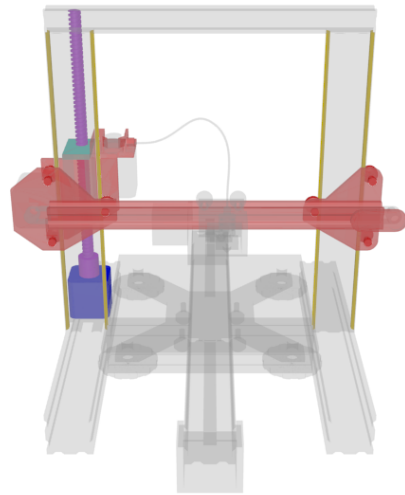
(b) 3D-model

Figure 6: The z-stage of the 3D-printer. a) is a photo taken from the left. It shows the stepper motor of the z-stage and how it is attached to the threaded rod. Also seen in the top right is a small portion of the moving part of the z-stage. b) is an approximate 3D-model, with the parts of the z-stage marked with different colors. The marked parts are the stepper motor (blue), the threaded rod (purple), the connection between the threaded rod and the moving part (cyan), the moving part (red) and the track the moving part moves on (yellow). The entire x-stage and extruder are attached to the moving part.

The z-stage (see figure 6) only provides movement between the different layers an object is made of. This movement needs to be more precise than the movement in the xy-plane, and the z-stage needs to be able to hold a position without deviation for extended periods of time. This is often achieved using a threaded rod attached to a stepper motor. Like the configuration of the xy-stage, exactly what this threaded rod moves can vary between printers. In the printer used in this paper, it moved the x-stage and extruder.

2.4.4 Extruder
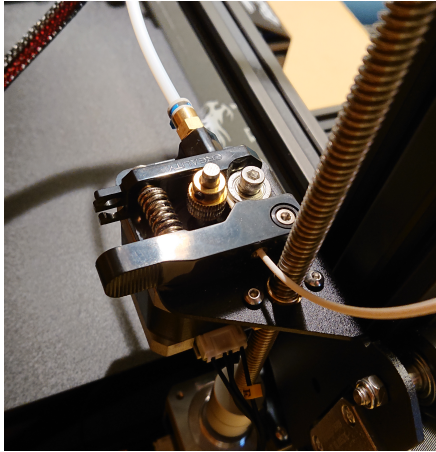
(a) Photo
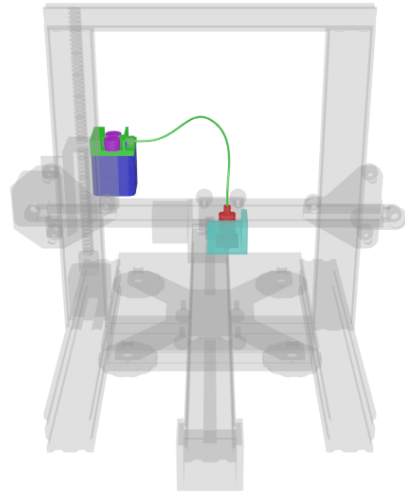
(b) 3D-model

Figure 7: The extruder of the 3D-printer. a) is a photo taken from the rear left. It shows the feeding mechanism of the extruder. A piece of white filament is in position to be fed by the mechanism. Also seen is a large portion of the threaded rod of the z-stage, as well as where it attaches to the moving part of the z-stage. b) is an approximate 3D-model, with the parts of the extruder marked with different colors. The marked parts are the stepper motor (blue), the toothed gear and roller that transfer movement from the motor to the filament (purple), the filament guide (green), the hotend (red) and the cooling fans (cyan). The nozzle (yellow) can barely be seen below the rest of the hotend (red).

The extruder consists of two major components: a feeder motor and a hotend, shown in figure 7. The feeder motor is a stepper motor, similar or identical to the ones used by the xyz-stage, that pushes material, in the form of a plastic filament, into the hotend using a toothed gear. The hotend is the part where the plastic that is to be extruded is molten. It ends in a small nozzle, that is used to precisely deposit the molten plastic to form the layers of the object that is being made. Near the hotend there is also often a fan that is used to cool and solidify the plastic that is coming out of the nozzle more or less rapidly.

The exact configuration of the extruder can again vary between different printers, in two major categories depending on how the feeder motor and hotend are connected. In one, the feeder motor is mounted directly to the hotend, pushing the filament directly into it without anything in between. In the other category, the feeder motor is connected to the hotend via a PTFE tube, with an inner diameter only barely above that of the plastic filament. This allows the feeder motor to be detached from the xy-stage, reducing the mass of the moving parts. The printer used in this paper used the latter type of extruder.

2.4.5 The printing process

Figure 8 shows a simple illustration of how a small rectangular cuboid is made with FDM. Differences between the intended shape (light grey) and the shape actually made (red and

blue) are exaggerated for improved clarity.

(a) Prior to deposition.   **(b)** Start of first layer.   **(c)** First layer finished.

(d) Ready for second layer.   **(e)** Start of second layer.   **(f)** Object finished.
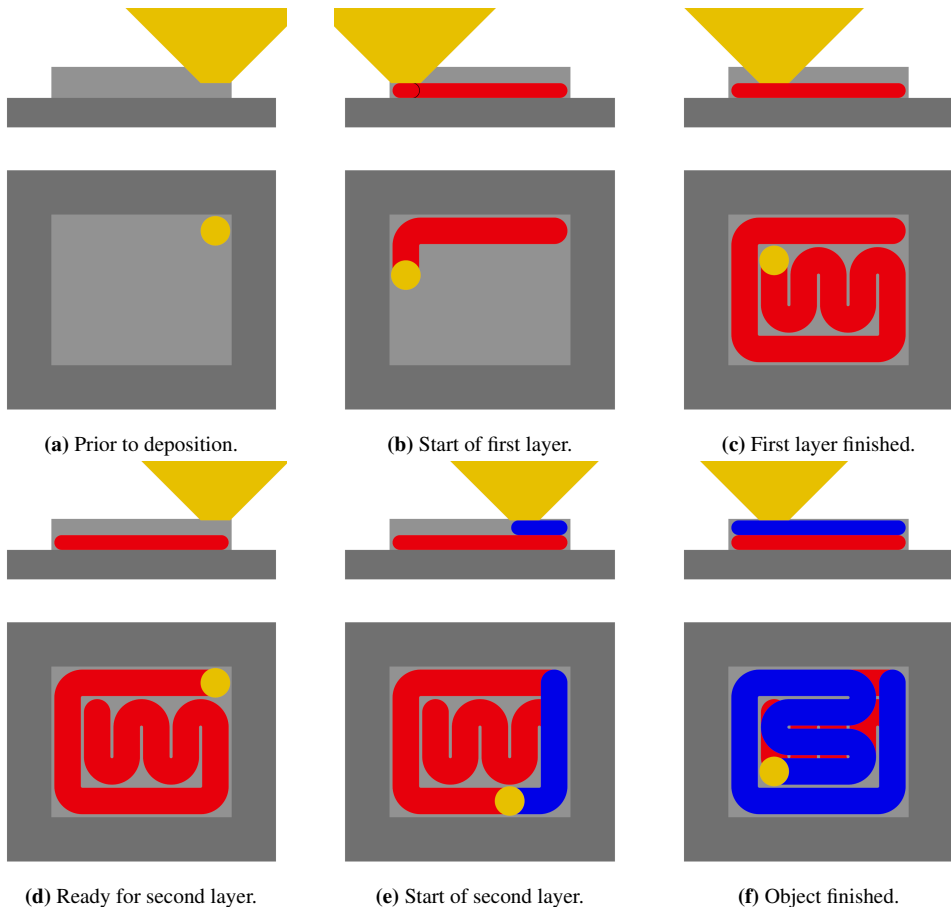
Figure 8: Two different views of the printing volume showing how the first layer of a cuboid is made with FDM. The parts shown are the print bed (dark grey), the shape of the object that is to be made (light grey), the extruder nozzle (yellow), the material of the first layer (red) and the material of the second layer (blue). a) shows the printing volume prior to any material being deposited. b) shows the printing volume right after the printing process has started. c) shows the printing volume when the first layer has just been completed. d) shows the printing volume immediately prior to the start of the second layer. e) shows the printing volume shortly after the second layer has been started. f) shows the printing volume when the second layer is finished and the object is complete.

When printing an object (or "making a print") with FDM, the printer starts with the extruder nozzle a fraction of a millimeter above the print bed (figure 8a). In a coordinated fashion the nozzle starts extruding molten plastic while the xy-stage starts moving the extruder around to fill in the first layer of the object that is being printed. Generally the perimeter of an object is printed first (figure 8b). As the plastic exits the nozzle it is quickly cooled and solidified by the surrounding air.

Once the first layer has been fully filled in (figure 8c), the z-stage moves the extruder up (or

the print bed down) a fraction of a millimeter (figure 8d) and the coordinated extrusion and movement starts filling in the next layer on top of the previous one (figure 8e). This is then repeated until the object is complete (figure 8f).

With this, FDM can be used to turn a 3D-model into a physical object. The 3D-model cannot however simply be given directly to the printer. It first needs to be turned into a series of commands that the printer can follow to make the object, commonly in the form of a .gcode file. The software used to make this conversion is often called a "slicer", since the first thing it does to a 3D-model is "slice" it into a series of thin layers. The slicer then plans a path for the printer to take to fill in each layer one by one.

2.4.6 Resolution

Stating the resolution of a FDM 3D-printer is not completely straightforward; there are at least three different values that could be argued to be the resolution: positioning resolution, print accuracy and nozzle size.

The positioning resolution comes from how many steps it takes the stepper motors to move the extruder a given distance. On the printer used in this paper the belt system in the xy-stage provides 80 steps/mm, while the threaded rod in the z-stage provides 400 steps/mm, resulting in a x × y × z resolution of 12.5 μm × 12.5 μm × 2.5 μm.

The print accuracy/precision/resolution on the other hand is not inherent to the hardware of the printer, but is rather a number provided by the manufacturer. It is the maximum amount that the dimensions of a printed object can deviate from those in the 3D-model it is based on. While this is not strictly a measure of resolution it is in many cases the closest thing to an officially stated resolution that is readily available. For the printer used in this paper the value given is 0.1 mm.

Lastly, the nozzle size is the size of the opening that molten plastic is extruded through. This determines the minimum size of the lines that the printer uses to fill in the layers objects are made from. This directly impacts the minimum size of positive features such as walls, but not negative features like channels (see figure 9). On the printer used in this paper the standard nozzle size is 0.4 mm, though this was changed as part of the experiments.
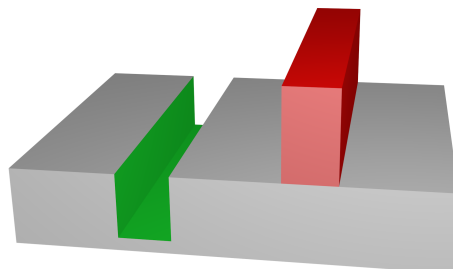

Figure 9: Simple 3D-model showing positive and negative features. The negative feature is green and the positive feature is red.

Only looking at the positioning resolution, FDM should theoretically be capable of making

sub-100 μm microfluidic channels quickly, without a mold, from the same thermoplastics used in mass production, while also being relatively cheap. Sadly reality is more complex than theory. Microfluidic channels made with FDM suffer from innumerable defects that affect the channel shape, as can be seen in figure 10. This restricts the minimum size of features that can be made consistently, the effective resolution, to something more similar to the print accuracy stated by the manufacturer.

0.1 mm

Figure 10: The actual shape of a sub-millifluidic channel made with FDM that was intended to be straight. The channel walls can be seen to have an undulating irregular shape.

2.5 Parameters that will be investigated

A 3D-model that is to be printed with FDM first needs to go through a slicer software before it can be given to the printer, to plan out how the printer will move. This planning is however far from simple. Due to the very physical nature of FDM printers, there are many mechanical flexibilities and elasticities that would cause severe defects in the printed object if left unchecked. To compensate for this, there are a large number of settings in the slicer software that can be used to fine-tune the printing process. The goal of this paper is to analyse what effect a small selection of these settings have on a microfluidic channel. Beyond these settings, the effect of one physical parameter of special interest, nozzle diameter, will also be investigated.

2.5.1 Nozzle temperature

The temperature of the nozzle is what determines the temperature, and through that the viscosity, of the molten plastic that is deposited by the print head. This means that it could feasibly affect any defects to the channel shape (see figure 10) that are caused by hydrodynamic effects.

The nozzle temperature also determines how well the deposited material fuses with previously deposited material below and beside it. This would have minimal effect on the channel shape, but it is quite crucial for making leak free channels and fully transparent

objects. It would thereby be positive if the nozzle temperature does not affect the channel shape, so that it can be adjusted freely for optimising for leak free and/or transparent channels.

2.5.2 Speed
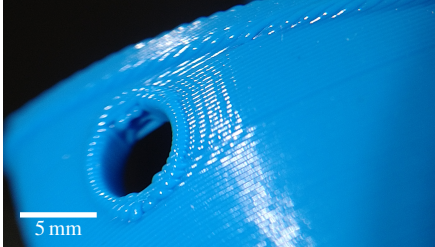
Figure 11: Photo showing how features, in this case a ring around a hole, can cause "ripples" in surfaces made with FDM, with a shape that mirrors the original feature. This phenomenon is called "ghosting".
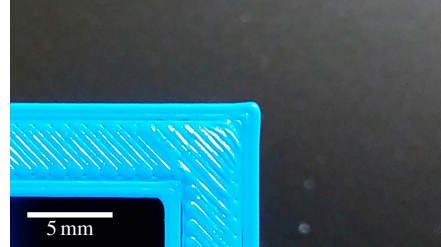
Figure 12: Photo of the corner of a simple square object made with FDM. The corner can be seen to not only be rounded, but actually spread outside the original square shape, forming a small "bump".

On larger scales, reducing the movement speed of the print head will essentially always improve print quality, with high print speed often leading to ghosting (see figure 11) and bumpy corners (see figure 12). It would be of interest to see if this relation between speed and quality holds true for small features, like microfluidic channels, as well.

2.5.3 Acceleration

Separate from speed, it is also possible to control the maximum acceleration of the print head. It is rarely changed, in favor of speed, but does also have a large effect on how the print head moves. Reducing it should in theory make velocity changes less sudden, which should reduce mechanical oscillations.

2.5.4 Layer height

Layer height is simply the thickness of the layers objects are made from. This only alters the height, and not the width, of the line of material the extruder deposits. As such, changing it should ideally not have any effect in the xy-plane. Changing it does however still affect the extrusion rate (the rate at which material is deposited). This means that, for example, reducing the layer height would reduce extrusion rate, which in turn would make the effect of absolute variations in extrusion rate more significant.

2.5.5 Fan speed

The fan speed affects the speed of the cooling fan that is used to cool the plastic more quickly once it has been extruded. Adjusting it should make it possible to solidify the plastic more or less immediately after coming out of the extruder nozzle, which should give some insight

into whether defects are present as soon as the plastic comes out of the nozzle or if they arise from interactions between the cooling plastic and its surroundings.

2.5.6 External perimeters first

Figure 13: Simple illustration of one layer of a cylinder with a hole in the middle made with FDM. The three basic types of lines of deposited material are shown in different colors. External perimeters are shown in red, internal perimeters are shown in yellow and infill is shown in blue.

This parameter determines whether or not the outermost perimeters (see figure 13) are made before the inner perimeters. This should be able to show if extruded material is affected by its in-plane surroundings, and if such effects can carry across to the other side of the extruded line.

2.5.7 Nozzle size

The size of the extruder nozzle, a physical parameter, has been suggested [18, 19, 20] to be something that needs to become smaller to make FDM more viable for making microfluidic devices. This is a reasonable hypothesis, since the nozzle size is what directly determines the minimum size of lines that can be deposited by the print head. Only positive features, such as walls and columns, are directly affected by this however. The connection to negative features, such as channels, is less certain. It is for example possible that undulations in lines that are intended to be straight, like those seen in figure 10, are caused by chaotic hydrodynamic behaviour and are proportional to the nozzle size. It is however also possible that such undulations are caused by mechanical vibrations, and are not connected to nozzle size at all.

3 Method

The FDM 3D-printer used for this paper was a Creality Ender-3 Pro, and the slicer software used to prepare 3D-models for printing was Ultimaker Cura. This specific printer was selected due to being the cheapest FDM 3D-printer available. Cheapness was prioritised to investigate what quality would be possible with a "low end" printer. Ultimaker Cura was used due to having a large number of different settings, including especially good separate control of the first layer.

3.1 Sample design

(a) 3D-view.

(b) 2D-view.
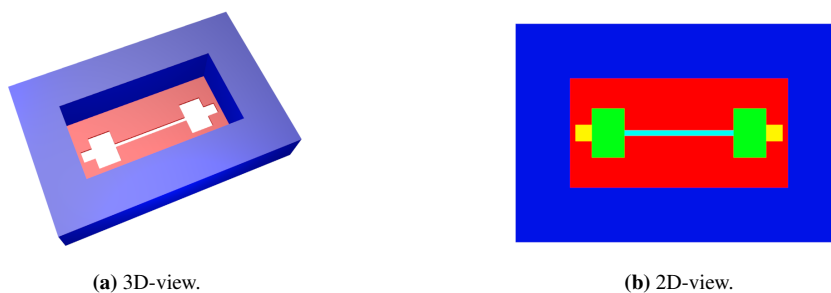
Figure 14: Illustrations of the "chips" that were made to test the effects of different parameters. The thin area (red) contains the "channel" (cyan), the structure used for the main measurements. The purpose of the surrounding structure (blue) was to maintain the structural integrity of the thin area and make it easier to handle the samples. The green areas are holes that provided access to the underlying surface for depth calibration. After such calibration the surface around the yellow area would then provide a smooth surface where the thickness of the red area could be measured.

(a) Angled view.

(b) From above.
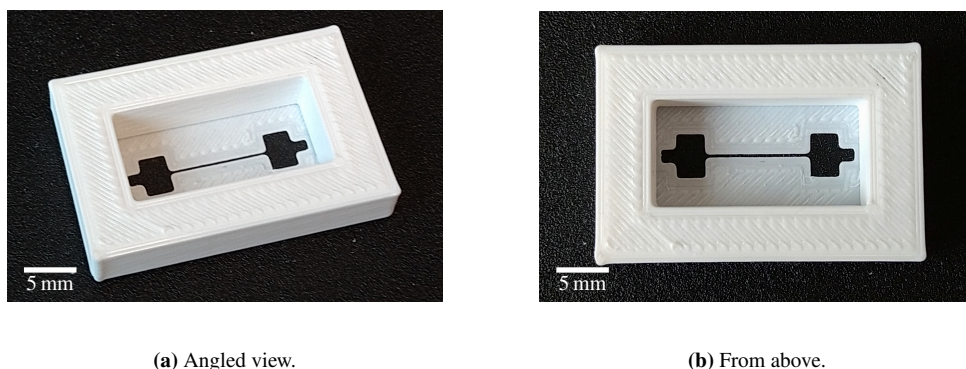
Figure 15: Photos of one of the "chips" used as samples.

To measure what effect changing the different parameters would have on a microfluidic channel, a special "chip" was designed (see figure 14 and 15). It consisted of two major structures: a thin area and a surrounding structure.

The purpose of the surrounding structure (seen in blue in figure 14) was to maintain the shape of the thin area and make the chip easier to handle.

The thin area (seen in red in figure 14) was always only present in the first 3D-printed layer of the chips. As such its thickness varied with the thickness of the first layer.

In the thin area there was a 0.4 mm wide and 10 mm long "channel" (seen in cyan in figure 14b), which was the part that was imaged and analysed to quantify the effects of the various parameters. It was essentially a microfluidic channel without a floor and ceiling. This lack of floor and ceiling was to make the walls of the channel easier to image and measure.

At each end of this channel there was a wider empty area, with the primary purpose of providing a clear start and end to the channel (green and yellow in figure 14b). It also enabled measurement of the thickness of this thin area, by providing places where a digital caliper could measure the vertical position of the top and bottom of the thin area.

This type of chip was printed for each of the combinations of settings, and would then act as the "sample" for that combination. To digitize the samples, the channel of each chip was micrographed in eleven different positions along the length of the channel using transmission microscopy. The eleven positions were evenly spaced 1.0 mm apart, and were consistent between chips.

Each micrograph only captured approximately 0.7 mm of the length of the channel. The result of this was that there were sections of the channel between micrographs that could not be seen, so the full length of the channels could not be seen in their entirety. This was not compensated for partly out of convenience and partly to ensure that no images overlapped.

3.2   Print bed calibration

An FDM 3D-printer cannot detect the position of the print bed while printing. If it is not exactly where the software of the printer expects it to be, the thickness of the first layer can deviate from the intended value and be inconsistent across an object. In the worst cases it can make the extruder nozzle scrape against the print bed, or result in the deposited material to not sticking to the print bed surface.

To avoid this, the print bed of FDM 3D-printers can usually be raised or lowered in three or four positions to calibrate it. The print bed of the Creality Ender-3 Pro has four such positions (see figure 3b). Here the print bed is held up by stiff springs, while a screw mechanism limits its maximum height. During normal use, the print bed will be held consistently at this maximum height by the springs. This spring, screw and wheel structure can be seen in figure 3a.

To minimize the variation caused by the manual calibration, it was always done in the four calibration spots in the same order. In each of these spots, the distance between the nozzle and print bed was measured by manually feeling how much friction they caused on a piece of paper as it was slid between them. To ensure that no residual plastic at the end of the nozzle affected the calibration, a flat piece of metal was held against the nozzle as it cooled after prints.

3.2.1 Calibration characterization

Since the calibration of the print bed was done manually, it would have some variation. To get a sense for how big this variation would be, the thickness of the first 10 chips was measured using the specially designed gaps (green and yellow in figure 14b) and a digital caliper. First the distance to the top of the first layer was measured, in the area that is yellow in figure 14b. With this as the zero point, the distance to the underlying surface, which should coincide with the bottom of the first layer, was measured in the area shown as green in figure 14b. The measurement positions can be seen in figure 16 and 17.
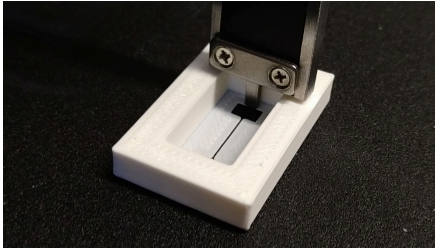
Figure 16: Photo showing how the distance from the top of the surrounding structure to the top of the first layer was measured.
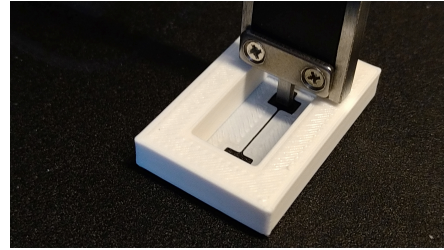
Figure 17: Photo showing how the distance from the top of the surrounding structure to the underlying surface, and through that the bottom of the first layer, was measured.

3.3 Print bed characterization
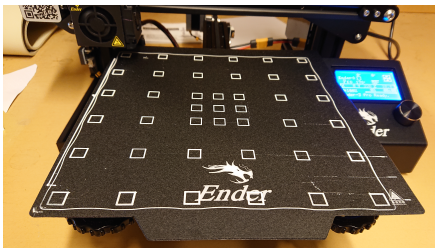
Figure 18: Photo of the print bed of the printer used in this paper after printing the grid of squares used to characterize the print bed.
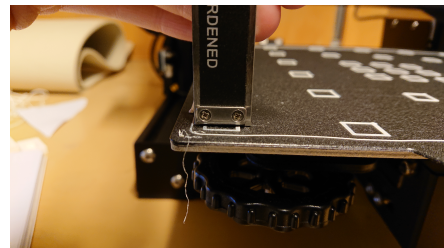
Figure 19: Photo showing how digital calipers were used to measure the depth of the squares used for characterization.

Since it was feasible that the distance between the print bed and nozzle could affect the shape of test channel, it was desirable to print the chips on a part of the print bed that had no tilt or other variation in height. To investigate this, a grid of squares one layer thick was printed across the print bed (seen in figure 18). Since the center of the print bed was the most likely place that the chips would be printed, simply because it is the default position, the grid was denser there. Once the squares had been printed, their thickness was measured using a digital caliper while still on the print bed, as seen in figure 19. Two such grids of squares were printed and measured.

3.4   Micrograph characterization

To ensure comparisons between intended dimensions and dimensions on the chips were accurate, the pixel to μm ratio in the micrographs was measured in both x and y using a micrometer.

3.5   Channel cleanness

To ensure that no dust contaminated the channels in the chips, they were moved directly from the print bed of the 3D-printer to the holder on the microscope, with the central thin area of the chips not touching any surfaces along the way.

3.6   Parameter ranges

The different parameters of interest were varied one by one across a range of different values. The structure of these ranges were not the same for all parameters; some varied exponentially and some linearly. For every parameter value one sample (per nozzle) was made. Additionally, 10 chips were made using standard settings with each nozzle, to provide a baseline.

- Nozzle temperature was varied linearly between 180°C and 220°C, which are on the lower and higher ends of the range of temperatures used for PLA in FDM.

- Speed varied exponentially between 0.5 and 2 of standard speed, which was 20 mm/s in this case.

- Acceleration limit was also varied exponentially, from 1 to 0.25 times normal, which was 400 mm/s^2. It was not varied above its normal value, since that would reduce the parameters effect and it is already nearly imperceivable at the normal value.

    - To exaggerate the effects of this variable, that is otherwise very subtle, the speed was set 40 mm/s rather than the standard 20 mm/s for the settings used to test acceleration.

- Layer height was varied linearly from 0.25 to 1 of the nozzle diameter (0.1 mm to 0.4 mm for the original nozzle).

- Fan speed was also varied linearly, from 0% to 100%.

- External perimeters first, being a binary choice was done at both its values, "yes" and "no". To provide more robust data, each value was done with speed set to 0.5, 1 and 2 of standard. This resulted in a total of 6 different combinations of parameters.

- Nozzle size was changed linearly, with the values 0.2, 0.4, 0.6 and 0.8 mm.

Parameters of special interest were investigated with multiple series of samples, made with different 0.4 mm diameter nozzles. Some series made with a 0.8 mm diameter nozzle were used as well.

3.7 Extruder nozzles used

The 3D-printer used in this paper originally had a nozzle with a diameter of 0.4 mm. To investigate the effect of nozzle diameter on the quality of microchannels, a separate set of four nozzles with diameters ranging from 0.2 mm to 0.8 mm, with the brand name PrimaCreator, were also used. For brevity, the following abbreviations will be used when referring to the different nozzles:

- O4: The original nozzle of the printer used, with a diameter of 0.4 mm

- P2: The PrimaCreator nozzle with a diameter of 0.2 mm

- P4: The PrimaCreator nozzle with a diameter of 0.4 mm

- P6: The PrimaCreator nozzle with a diameter of 0.6 mm

- P8: The PrimaCreator nozzle with a diameter of 0.8 mm

4 Results and discussion

Figure 20 shows the typical appearance of one of the test channels. Note that the "vertical channels" are not actual channels, but artifacts from the data collection method. How the micrographs are positioned relative to the full channel can be seen in figure 21.

Figure 20: The eleven micrographs of one sample placed in series to show the appearance of the full length of the channel. Note that the "vertical channels" are artifacts of the data collection process. The actual channels made were simple continuous channels with no form of side channels.
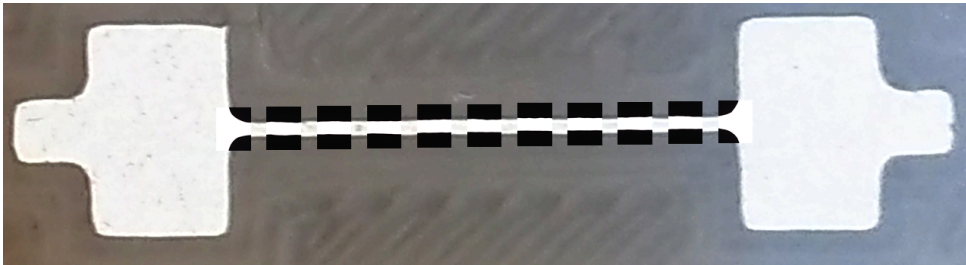
Figure 21: The eleven micrographs of one sample shown on top of a photo of the same channel. As can be seen, there are spaces between adjacent micrographs.

Standard analysis of all datasets resulted in around 120 different graphs. As such showing every graph would make the "Results and discussion" section unreasonably long. Instead, only the graphs where there seems to be a possible correlation between the property measured and the parameter varied will be shown.

Since the focus is on analysing the effects on a straight segment of microfluidic channel, only the central 5 mm is used in the main analysis, to avoid the results being dominated by the bumps present at the end of the test channels, seen in figure 22.

Figure 22: The eleven micrographs of one sample placed in series to show the appearance of the full length of the channel. This channel in particular has significant deflections in channel shape at the start and end of the channel. Note that the "vertical channels" are artifacts of the data collection process. The actual channels made were simple continuous channels with no form of side channels.

4.1 Channel properties measured

The following channel properties were determined for each chip. The properties were then plotted against the various parameters to look for correlations.

4.1.1 Average channel width

"Average channel width" is the average width of the channel of one chip. It would ideally have a value of 400 μm, since that is the width the channels are intended to have.

4.1.2 Channel width deviation

"Channel width deviation" describes how much the channel width varies within one channel. It includes both standard deviation and maximum deviation. This is an important measure, since it shows how close the channel is to an ideal perfectly straight channel. A low value indicates that a channel has a more consistent width.

4.1.3 Channel offset deviation

"Channel offset deviation" describes how much the position of the central line of the channel varies within one channel. It includes both standard deviation and maximum deviation. "Channel offset deviation" is complementary to "Channel width deviation" as they come from addition and subtraction, respectively, of the position of the channel sides. A low value indicates a more straight channel, which is the intended shape.

4.1.4 Channel width at end bumps

"Channel width at end bumps" analyses the "bumps" sometimes present at the ends of channels in the chips, like the ones seen in figure 22. Specifically it measures how much the channel width in the gap between the edge-most and second to edge-most images differs from the channel average, by taking the average channel width on the edges of images closest to this gap. Negative values indicate that the channel is narrower at these bumps, while positive values indicates that it is wider. As such an ideal value would be 0, since that would suggest that the channel width is unaffected by these bumps.

This is a quantitative measure of the previously discussed bumpy corners that can be noticeable on macroscopic objects (see figure 12). The width of the channels tended to deviate the most in these areas, so keeping these kinds of bumps in check would be important for ensuring that microfluidic channels are open.

4.1.5 Fourier transform of upper edge of channel

"Fourier transform of upper edge of channel" is the average of a spatial, rather than temporal, Fourier transform of the upper side of the channel in the individual images. For each image, a Fourier transform was done of the position of the upper side as a function of the position along the length of the channel (horizontal in figures), rather than as a function of time. This was then added together with the Fourier transforms from the other images of the same chip, to acquire the average spatial Fourier transform for that chip. The Fourier

transform for all chips made was found to consistently be quite similar. To highlight variations, the average Fourier transform for each chip was divided by a compensatory function (see figure 23a) prior to being displayed as a heatmap (see figure 23b).

The spatial Fourier transform would help distinguish if there are any regular patterns in the shape of the channel, similar to how a temporal Fourier transform can distinguishing regular patterns (frequencies) in a signal. A larger feature size would also indicate that the shape of the channel changes more slowly.

(a) Line graph   **(b)** Heatmap
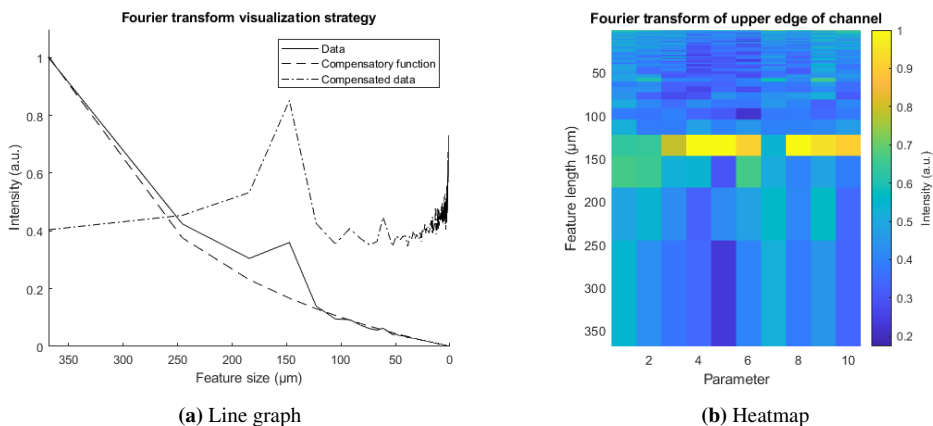
Figure 23: a) is a graph showing how the data from the Fourier transform of the channels was prepared before being displayed as a heatmap. b) is such a heatmap. Note that both graphs have especially high intensity around a feature size of 150 μm.

4.1.6 Average distance between peaks and valleys on the channel sides

"Average distance between peaks and valleys on the channel sides" measures the average distance between the local maxima and minima, or peaks and valleys, of the position of the channel sides. Figure 24 shows an example of these peaks and valleys. This gives information similar to previously described Fourier transform, but should be more capable of resolving features with lengths similar to the span of one image. A larger average distance would indicate that the shape of the channel changes more slowly, which would be closer to the ideal case of no change at all.
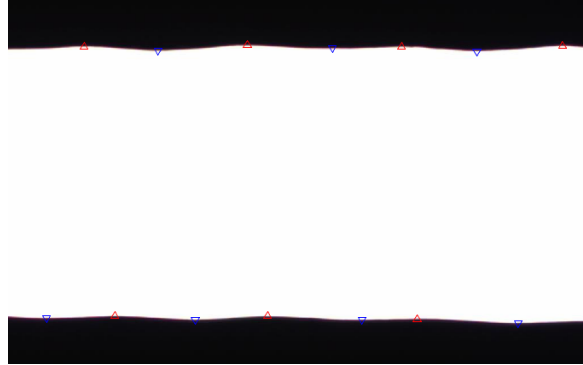
Figure 24: A part of a channel with the "peaks" of the sides marked with red triangles and the "valleys" marked with blue triangles.

4.1.7 Average pixel plateau length

The pixelated nature of the data makes the calculated positions of the channel sides change in very discrete steps. This makes a direct derivative becomes less useful,since it can essentially only have one of two different values (0 or 1, see figure 25b). "Average pixel plateau length" instead looks at the plateaus these steps create, measuring their average length. This is similar to an inverse derivative, with larger plateaus indicating a slower rate of change, which would be closer to the ideal of no change.

(a) Full channel width.

(b) A small portion of a).
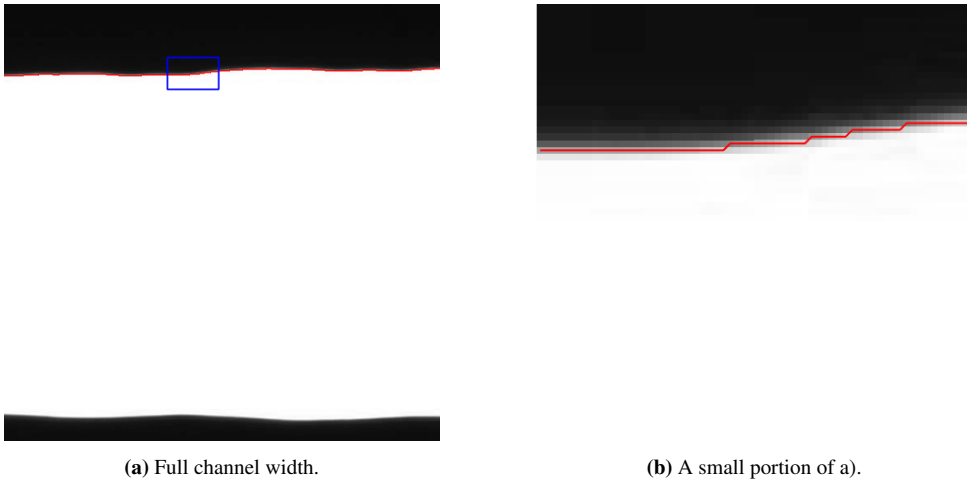
Figure 25: Micrographs at different zoom levels. The calculated position of the upper edge of the channel is shown in red. a) shows the full width of a channel, with a fraction of the upper edge marked by a blue border. b) shows the area that is within the blue border in a), clearly showing how the calculated position of the channel edge consists of a series of plateaus, due to the pixelated nature of the image.

30

4.2 Nozzle temperature

Nozzle temperature could feasibly influence the quality of the chips since it affects the viscosity of the molten plastic as it is extruded. If such an influence exists it would however make improving the general quality of microfluidic devices made with FDM more complicated, since nozzle temperature is also a crucial parameter in controlling the transparency and structural integrity of objects printed with FDM.

Two series of samples that investigated nozzle temperature were made, one using nozzle O4 and the other using nozzle P4. For both series the first sample, with an extruder temperature of 180 °C, failed to print. This was likely due to the low temperature making the viscosity of the molten plastic too high for the 3D-printer to extrude. The other eight samples, with temperatures ranging from 185 °C to 220 °C, were however printed successfully.

4.2.1 Average channel width vs nozzle temperature

(a) Data from nozzle O4.   (b) Data from nozzle P4.
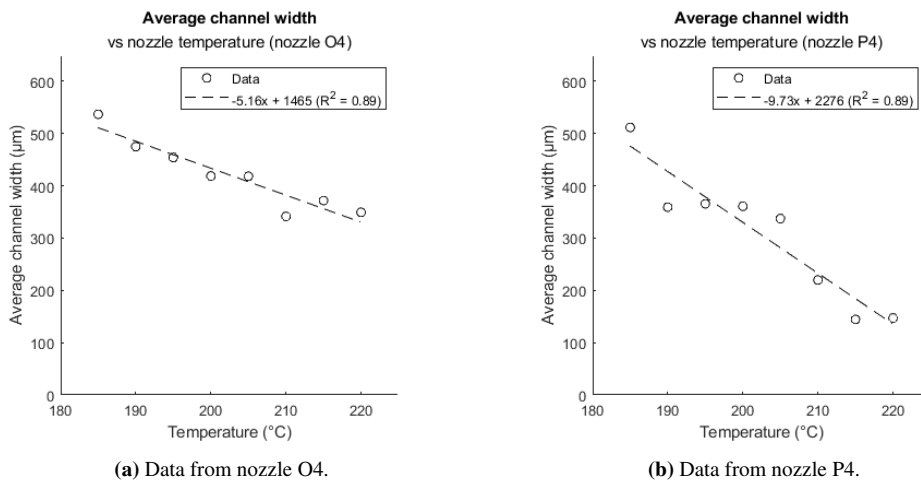
Figure 26: Graphs showing how average channel width varied with temperature. A linear fit has been added to enable easy comparison between different graphs. a) shows the data that was acquired from samples made with nozzle O4, while b) shows the data that was acquired from samples made with nozzle P4.

The average channel width varied heavily even within samples made using the same set of settings. Nonetheless figure 26 seems to show a correlation between nozzle temperature and channel width, with a higher temperature leading to a more narrow channel. This correlation could quite possibly be due to the reduced viscosity of the molten plastic allowing it to deform and spread out more. Since this would affect the cross-sectional profile of the "channel walls", cross-sections could likely be a good way of investigating such an effect further. Understanding of such a phenomenon could be useful in trying to make channel walls made with FDM more vertically smooth, since they normally have a quite pronounced micro-scale structure.

It is also possible that the correlation between nozzle temperature and average channel width

is caused by the reduced viscosity making it easier for the molten plastic to flow through the extruder nozzle. If this flow is slightly hindered under normal printing conditions, reducing the viscosity of the molten material would allow the extruder to deposit slightly more material, resulting in a more narrow channel. This would match with the correlation seen in the data.

4.2.2 Channel width at end bumps vs nozzle temperature

(a) Data from nozzle O4.   (b) Data from nozzle P4.
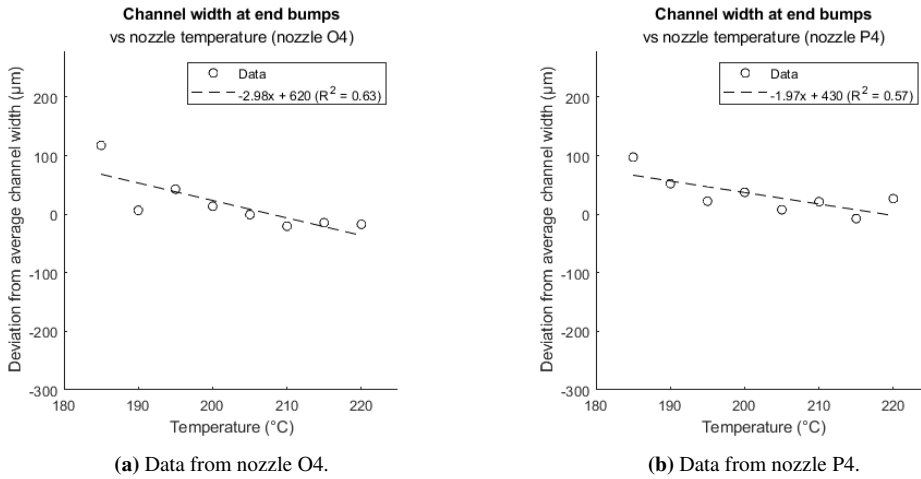
Figure 27: Graphs showing how the change in width of the channel near the openings varied with temperature. A linear fit has been added to enable easy comparison between different graphs. a) shows the data that was acquired from samples made with nozzle O4, while b) shows the data that was acquired from samples made with nozzle P4.

Figure 27 shows a similar correlation between nozzle temperature and the channel width at the end bumps, with higher temperature causing the channel to be narrowed more by them. It seems quite possible that this correlation is caused by the same effect that causes the correlation with average channel width, with the effect being slightly stronger at the corners.

4.3 Speed

Reduced speed is often associated with increased macro-scale quality when using FDM, so it is of interest to see if this holds true on micro-scale as well. A requirement for low speed would however also limit how quickly microfluidic devices can be made with FDM.

Three series of samples that sought to analyse the effect of speed were made, using nozzle O4, P4 and P8.

4.3.1 Average channel width vs speed

**(a)** Data from nozzle O4. **(b)** Data from nozzle P4. **(c)** Data from nozzle P8.
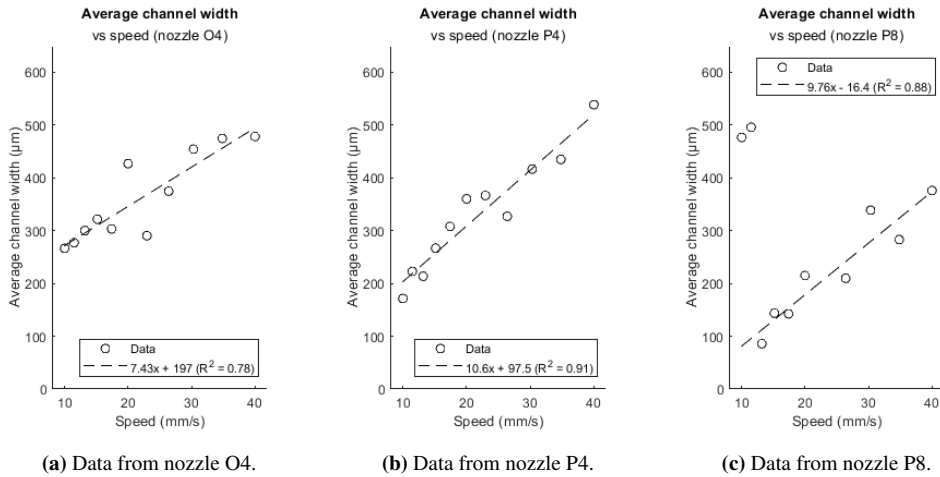
Figure 28: Graphs showing how average channel width varied with movement speed. A linear fit has been added to enable easy comparison between different graphs. a) shows the data that was acquired from samples made with nozzle O4, b) shows the data that was acquired from samples made with nozzle P4 and c) shows the data that was acquired from samples made with nozzle P8.

Figure 28 appears to show a clear positive correlation between speed and average channel width, with the exception of a number of outliers. If there is sufficient hydraulic resistance in the extruder nozzle to hinder extrusion under normal conditions, this could be caused by the increased speed making it more difficult for the extruder to deposit enough material. This would result in the line of deposited material being slightly more narrow, which would lead to a wider channel. While this would normally be a factor that would need to be compensated for, it could possibly be used for fine control of the channel width if the position resolution is insufficient.

Another possibility is that increased speed offsets the path that the extruder takes to make the channel, affecting the channel width through that. This does however seem unlikely for a number of reasons. If the increased speed caused the stepper motors to jump a step, the change in channel width should occur in discrete steps and it should make a distinct sound during the printing process. Meanwhile, if the speed caused some form of offset in the mechanical system of the movement axes it should cause some form of noticeable gradual drift. In either case, the symmetry of the chip should cause there to be equal numbers of widening and narrowing offsets, which should cancel out the effect.

4.3.2 Channel width at end bumps vs speed

**(a)** Data from nozzle O4. **(b)** Data from nozzle P4. **(c)** Data from nozzle P8.
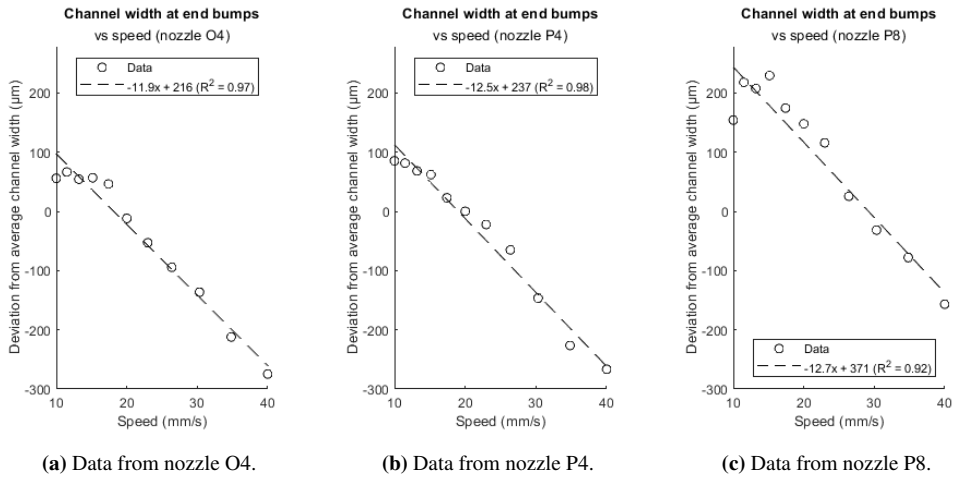
Figure 29: Graphs showing how the change in width of the channel near the openings varied with movement speed. A linear fit has been added to enable easy comparison between different graphs. a) shows the data that was acquired from samples made with nozzle O4, b) shows the data that was acquired from samples made with nozzle P4 and c) shows the data that was acquired from samples made with nozzle P8.

Figure 29 shows a quite clear correlation between how wide the channel is at the end bumps and the movement speed. This is not a too surprising result, since these bumps are believed to be caused by the momentum of the extruder causing it to "overshot" as it makes the 90° turn at the start of the channel. There are however bumps at all four corners of the channel, of which the momentum mechanism could only cause two. Two of them are in fact larger, so the momentum mechanism likely still has an effect.

Something that would cause bumps at all corners and increase at greater speeds would be over-extrusion at the corners. As the extruder approaches a corner, it slows down to reduce the previously mentioned momentum bump. The flow of material cannot be changed quickly enough to compensate for this however, since the molten plastic is somewhat compressible and will store some pressure. The result of this would be over-extrusion at the corners, with the excess material spreading out and making a bump. At higher speed, the flow of material would be greater, and the extruder would need to spend more time accelerating and decelerating, causing more total over-extrusion and larger bumps.

The correlation does however not only show that the channel can be narrower at the end bumps, but wider as well. This could be due to there being some form of compensatory mechanism for these end bumps in the slicer or printer, that ends up overcompensating at low speeds. There could also be some separate effect that causes this widening, that becomes more prominent when the low speed reduces the size of the bumps.

Interestingly, the widening is more significant when using a wider nozzle. This suggests that optimal movement settings not only depend on the structure of the 3D-printer, but on

the nozzle size as well. Further analysis of this could also provide a window into the mechanics of these bumps, using for example more detailed examination of their shape.

4.3.3 Average distance between peaks and valleys vs speed

(a) Data from nozzle O4.　　　**(b)** Data from nozzle P4.　　　**(c)** Data from nozzle P8.
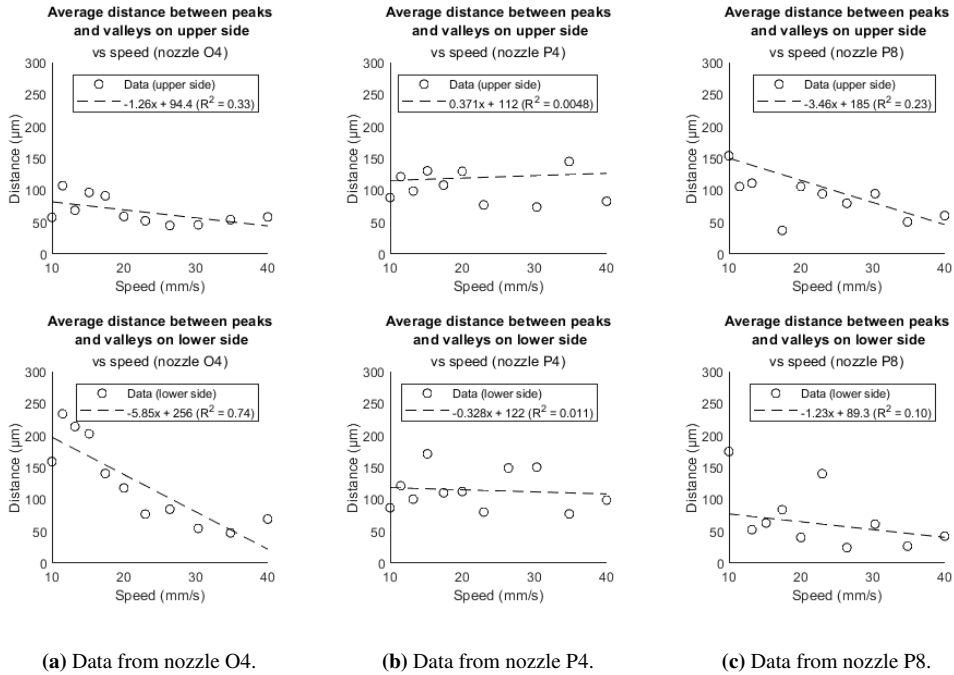
Figure 30: Graphs showing how the average distance between peaks and valleys in the shape of the channel sides varied with movement speed. A linear fit has been added to enable easy comparison between different graphs. a) shows the data that was acquired from samples made with nozzle O4, b) shows the data that was acquired from samples made with nozzle P4 and c) shows the data that was acquired from samples made with nozzle P8.

Figures 30a and 30c seem to show some form of negative correlation between the average distance between peaks and valleys and speed, while figure 30b does not seem to show such a correlation. While a correlation between speed and average distance between peaks and valleys would not be too surprising if the cause for the peaks and valleys is dependent on time, it is the opposite of what would be expected from for example time dependent vibrations. This will be expanded upon in section 4.3.4.

The correlation seen does on the other hand fit with the idea that low speed is good, since it would suggest that the variation in the channel shape occurs more slowly at low speed. This in turn would bring it closer to the ideal of no variation at all. It is however also possible that the apparent correlation is only caused by random chance, since there is some clear random variation present in them and only two of the three series of samples actually support it.

4.3.4 Average pixel plateau length vs speed

(a) Data from nozzle O4.　　　**(b)** Data from nozzle P4.　　　**(c)** Data from nozzle P4.
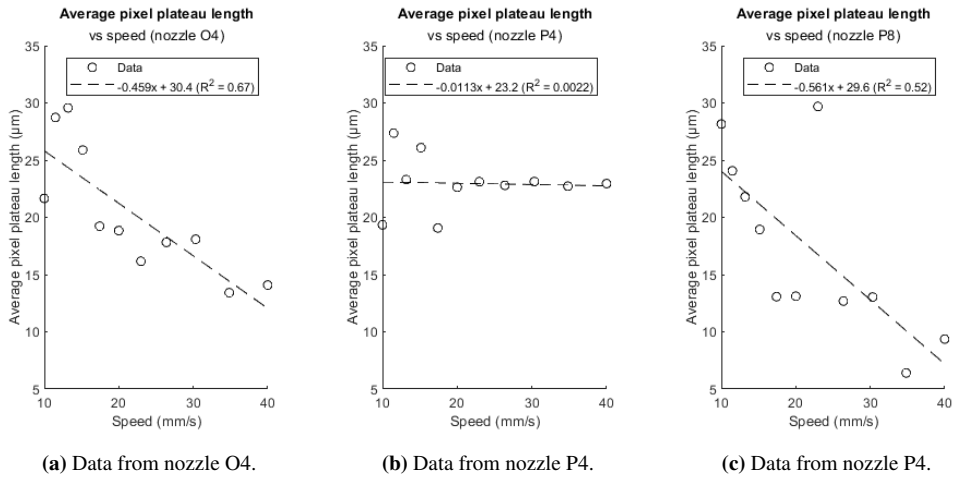
Figure 31: Graphs showing how the average pixel plateau length change varied with movement speed. A linear fit has been added to enable easy comparison between different graphs. a) shows the data that was acquired from samples made with nozzle O4, b) shows the data that was acquired from samples made with nozzle P4 and c) shows the data that was acquired from samples made with nozzle P8.

Similar to what is seen with the distance between peaks and valleys, figure 31a and 31c seem to show a correlation between average pixel plateau length and speed. Figure 31b does however again seem to lack a correlation. Such a correlation would also suggest that low speed provides better quality, as the shape of the channel would change more slowly. It is however uncertain if the correlation actually exists or if it is caused by chance.

While two of the three series of samples support that low speed causes the shape of the channel to change more slowly, specifically these two is a surprising pair. One series was made with the original nozzle of the printer (figure 30a and 31a), while the other was made with the Prima 0.8 mm nozzle (figure 30c and 31c). While the other two possible pairings could be explained by some relation to nozzle size or nozzle manufacturer, the present pair does not have anything immediately obvious in common.

If the correlation nonetheless does exist, it does not seem to be caused by time dependent or space dependent vibrations. If the variations were caused by some time dependent phenomenon there should be more space between them at high speed, while if they were caused by a phenomenon that depends on spatial position the distance between variations should not depend on speed. The data does however not fit either of these, with variations being closer together at high speed. This means that the variations are not caused by time dependent mechanical vibrations or some form of physical unevenness. This would leave stress dependent vibrations, the electronic control system and fluid mechanics in the extruder nozzle as possible causes for these variations in channel width.

4.4 Acceleration

Acceleration provides a limit on the maximum rate of acceleration for the extruder nozzle, which should in theory limit the forces applied to it and the structure of the 3D-printer. This does also affect the average speed of the printer, especially at lower acceleration limits.

Three series of samples investigated the effect of limiting the acceleration, made using nozzle O4, P4 and P8.

4.4.1 Channel width deviation vs acceleration

(a) Data from nozzle O4.   **(b)** Data from nozzle P4.   **(c)** Data from nozzle P8.
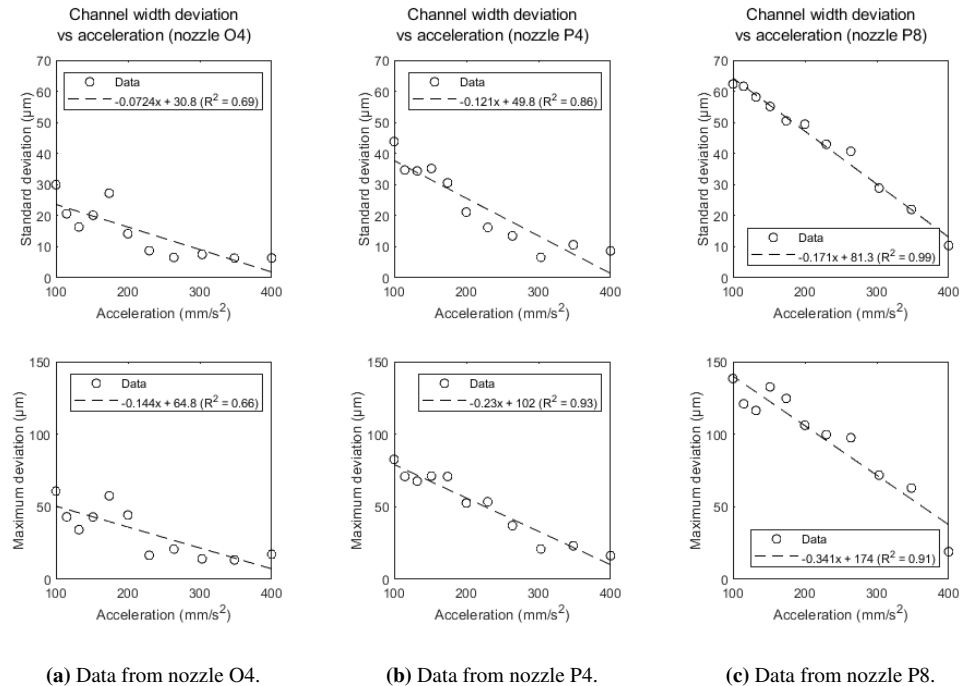
Figure 32: Graphs showing how the standard and maximum deviations of the channel width varied with maximum allowed acceleration. A linear fit has been added to enable easy comparison between different graphs. Note that the y-axis ranges are not the same as in other graphs of these channel properties. a) shows the data that was acquired from samples made with nozzle O4, b) shows the data that was acquired from samples made with nozzle P4 and c) shows the data that was acquired from samples made with nozzle P8.

The standard and maximum deviations of the channel width turned out to be surprisingly immutable, being dominated by random variation. The only parameter where this was not the case was acceleration, as can be seen in figure 32. The way in which acceleration affected the standard and maximum deviations of the channel width was however unexpected; a lower acceleration limit, that should reduce the general forces and stresses in the printer, heavily increased the standard and maximum deviations. A closer examination of the data did however show that this was not mainly due increased unevenness in the channel, but

instead due to the residual deviation from the end bumps creeping further and further towards the lengthwise middle of the channel, seen in figures 33 and 34. This is however still a quite surprising result; making the extruder change direction more gently causes the negative effects of this change in direction (bumps at the ends of the channel) to become more significant. This very strongly suggests that these problematic bumps are not actually caused by the extruder deviating from its intended path.

Combining the results from the tests of speed and acceleration seems to suggest that at least a significant part of the bumps at the end of channels are caused by time spent accelerating, rather than the magnitude of acceleration or total change in velocity. This would fit with the idea that the bumps are caused by that the rate at which the extruder deposits material is unable to keep up with the change in speed, resulting in over-extrusion when the movement of the extruder slows down. This will be discussed in more detail in General discussion.

Figure 33: The eleven micrographs of one sample placed in series to show the appearance of the full length of the channel. This sample was made with a speed of 40 mm/s and an acceleration of 400 mm/s^2, with all other settings at their standard values. A grey straight line is shown on each side of the channel to make it easier to see how the channel deviates from this straight line. Note that the "vertical channels" are artifacts of the data collection process.

Figure 34: The eleven micrographs of one sample placed in series to show the appearance of the full length of the channel. This sample was made with a speed of 40 mm/s and an acceleration of 100 mm/s^2, with all other settings at their standard values. A grey straight line is shown on each side of the channel to make it easier to see how the channel deviates from this straight line. Note that the "vertical channels" are artifacts of the data collection process.

4.5   Layer height

Layer height determines the thickness of the layers that a 3D-printer uses to make objects. It is often associated with quality, since a smaller layer height is directly related to vertical resolution. A smaller layer height does however also mean that it takes longer to make objects, since it increases the total number of layers the 3D-printer needs to make.

Three series of samples investigated the effect of layer height, one with the original 0.4 mm nozzle, one with the Prima 0.4 mm nozzle and one with the Prima 0.8 mm nozzle. To get the actual layer height, rather than just the intended one which had been found to vary

a lot from the actual one, the thickness of the first layer of the chips was measured using the procedure described in section 3.2.1. As a result of this, the relative difference between consecutive measurements varied significantly. In one case the deviation from the intended layer height even caused a data point to have a lower, instead of higher, layer height compared to the previous data point, resulting in them swapping order. This swapped order can be seen in figures 35c and 36c.

4.5.1 Channel width and offset deviation vs layer height

(a) Data from nozzle O4. **(b)** Data from nozzle P4. **(c)** Data from nozzle P8.

Figure 35: Graphs showing how the standard and maximum deviations of the channel width varied with layer height. a) shows the data that was acquired from samples made with nozzle O4, b) shows the data that was acquired from samples made with nozzle P4 and c) shows the data that was acquired from samples made with nozzle P8.

(a) Data from nozzle O4.   **(b)** Data from nozzle P4.   **(c)** Data from nozzle P8.
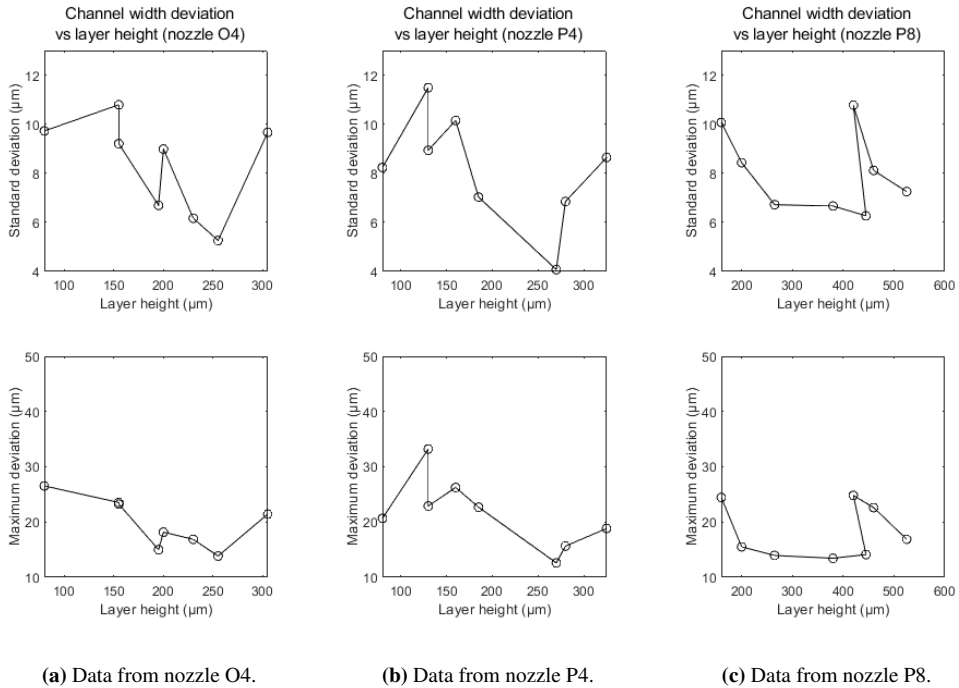
Figure 36: Graphs showing how the standard and maximum deviations of the channel offset varied with layer height. a) shows the data that was acquired from samples made with nozzle O4, b) shows the data that was acquired from samples made with nozzle P4 and c) shows the data that was acquired from samples made with nozzle P8.
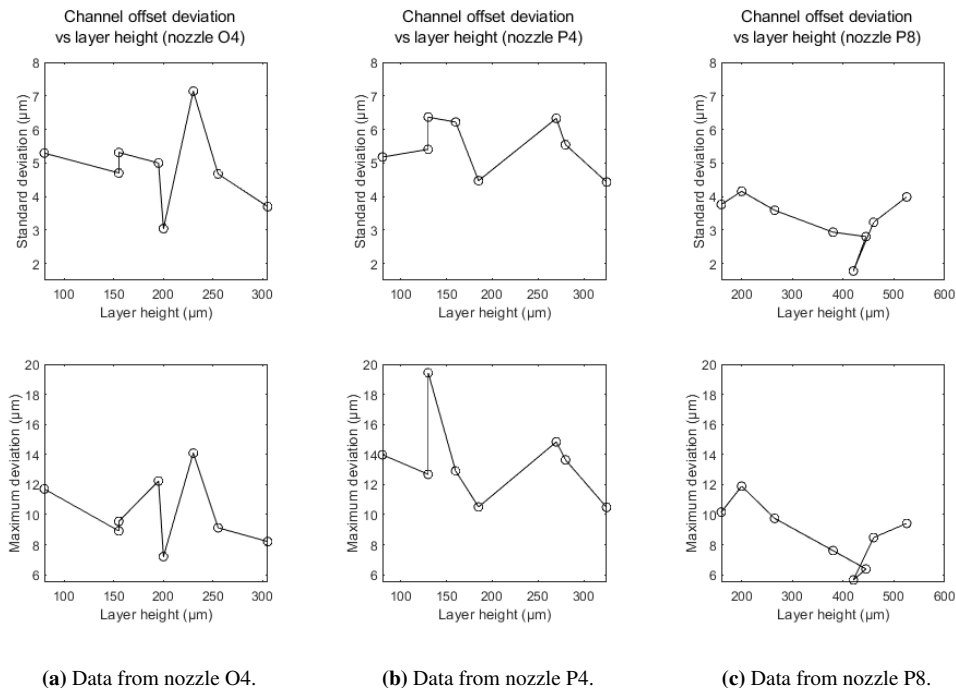
While figures 35 to 36 have significant amounts of random variation in the data, they are still interesting due to the significance of what they suggest. While it might take some imagination, it could be argued that they all have a local minimum. If these minima are taken as true, it would mean that with proper adjustment of layer height it would be possible to use a Creality Ender-3 Pro to make microfluidic channels with a width that does not deviate by more than 15 μm, and mostly does not deviate by more than 6 μm. This would bring the effective resolution of the printer close to its theoretical maximum of 12.5 μm. While the results here are far from significant enough to confirm this, they do show that this is something that needs to be investigated further.

Since it is important for a usable microfluidic channel to have a constant or at least predictable width, the seemingly random heavy variation often seen in channels made with FDM is a significant hindrance to the manufacturing method being viable for making microfluidic devices. The data presented in figure 35 to 36, if taken at face value, suggests that such variation could be consistently reduced to less than 15 μm. While this is crude compared to the accuracy of soft lithography, it would make it possible to make truly microfluidic channels with FDM with relative ease. Combining this with the cheapness and wide variety of materials available could make FDM an important tool for rapid prototyping of microfluidic devices. This is however only if the correlation between layer height and the standard and maximum deviation of channel width and offset actually exists; more reserach

is needed to confirm if this is really the case.

Identifying a possible mechanism for this correlation between layer height and channel deviations is more difficult, especially with the less than optimal data. Considering that the local minimum seems to be around half of the nozzle diameter, it is likely related to the specific microfluidic environment between the nozzle and print bed, but again more research is needed.

4.5.2 Channel width at end bumps vs layer height

(a) Data from nozzle O4.   **(b)** Data from nozzle P4.   **(c)** Data from nozzle P8.
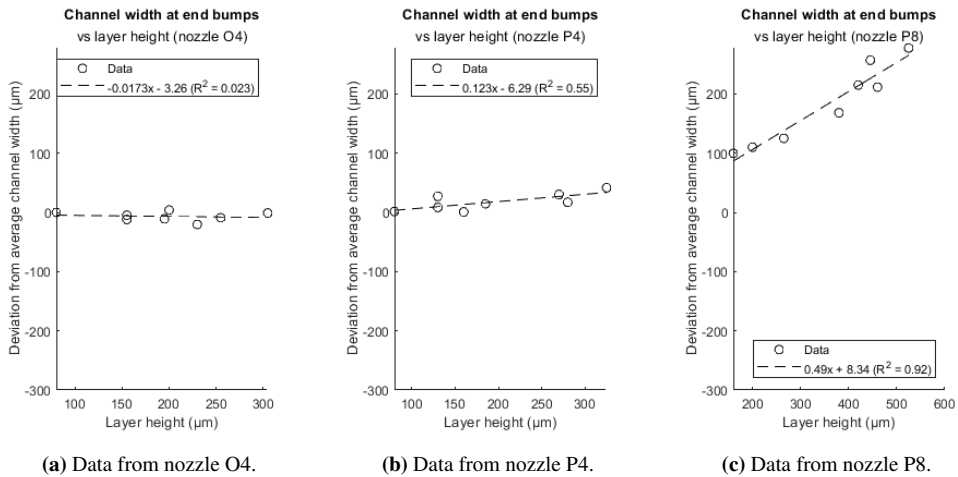
Figure 37: Graphs showing how the change in width of the channel near the openings varied with layer height. A linear fit has been added to enable easy comparison between different graphs. a) shows the data that was acquired from samples made with nozzle O4, b) shows the data that was acquired from samples made with nozzle P4 and c) shows the data that was acquired from samples made with nozzle P8.

Though it is only present in figure 37b and 37c, both of which are based on samples made using nozzles from the same manufacturer, there does seem to possibly be a positive correlation between the width of the channel at the end bumps and the layer height. Oddly, this correlation also seems to become more clear with successive series of samples (nozzle O4 was used first, nozzle P8 was used last). Interestingly, for the two series where there is a correlation the channel is consistently wider at the end bumps, while it tends to be narrower in the one series that does not have a correlation.

Such a correlation could be caused by increased layer height somehow providing more vertical room for the material of the bump to move in, reducing how far it spreads in the xy-plane. This does however seem somewhat unlikely; if anything the reduction of the total amount of material deposited for thinner layers and the greater hydraulic resistance to spreading between the nozzle and print bed should reduce the size of the bumps at low layer heights, rather than the opposite.

4.5.3 Average pixel plateau length vs layer height

(a) Data from nozzle O4.　　**(b)** Data from nozzle P4.　　**(c)** Data from nozzle P8.
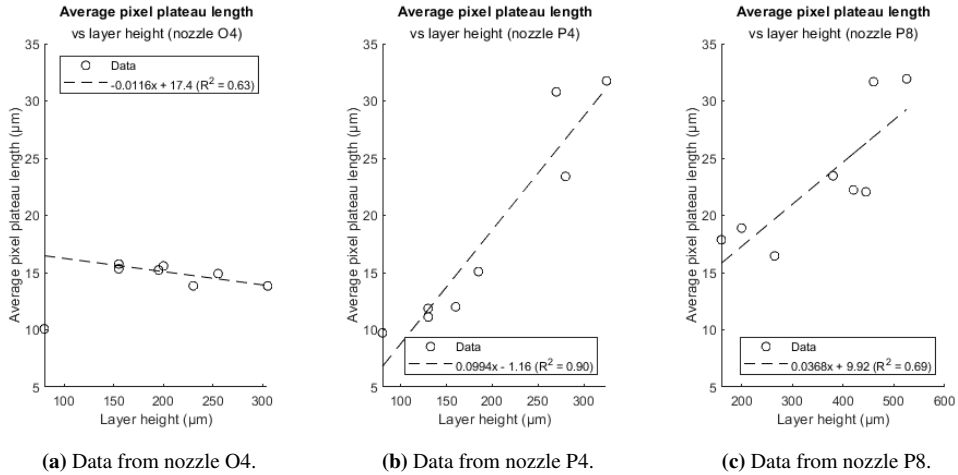
Figure 38: Graphs showing how the average pixel plateau length change varied with layer height. A linear fit has been added to enable easy comparison between different graphs. a) shows the data that was acquired from samples made with nozzle O4, b) shows the data that was acquired from samples made with nozzle P4 and c) shows the data that was acquired from samples made with nozzle P8.

Similar to what is seen with the channel width at the end bumps, figure 38b and 38c seem to show a correlation between average pixel plateau length and layer height in two of the three series. Here the correlation does however not become successively more clear. Oddly the series that does not match the other two instead has a negative correlation, though with an unusually prominent outlier.

A positive correlation between layer height and average pixel plateau length would not be too surprising, if scaling the deposited material up in the vertical direction (increasing layer height) could feasibly also scale it up in the horizontal direction (elongating it in the lengthwise direction). This should however also, in a simplistic view, scale up the variations in the widthwise direction too, something that does not appear to happen since the channel width standard and maximum deviations are unchanged.

4.6 Fan speed

Fan speed determines how rapidly the molten plastic deposited by the extruder is cooled, by controlling the speed of a cooling fan directed at the extruder nozzle. While it is important for bridging (crossing gaps without support), it generally does not have any effect on the shape of makro-scale objects. It could however still feasibly affect micro-scale quality if the shape of deposited material changes between being deposited and fully solidifying. The fan speed did however not seem to have any correlation with any of the measurements described in section 4.1.

4.7 External perimeters first

External perimeters first is a parameter that is quite different from all other parameters investigated in this report. It is a binary choice and does not affect any physical properties of the printing process, but rather how it is organized. As its name suggests it determines if the external perimeters, in this case the part of the wall exposed to the inside of the channel (see figure 13), are printed first. To provide more than one datapoint per option (yes or no) per measure, the speed was varied between three different values for each option.

4.7.1 Channel width and offset standard deviation and average channel width vs external perimeters first
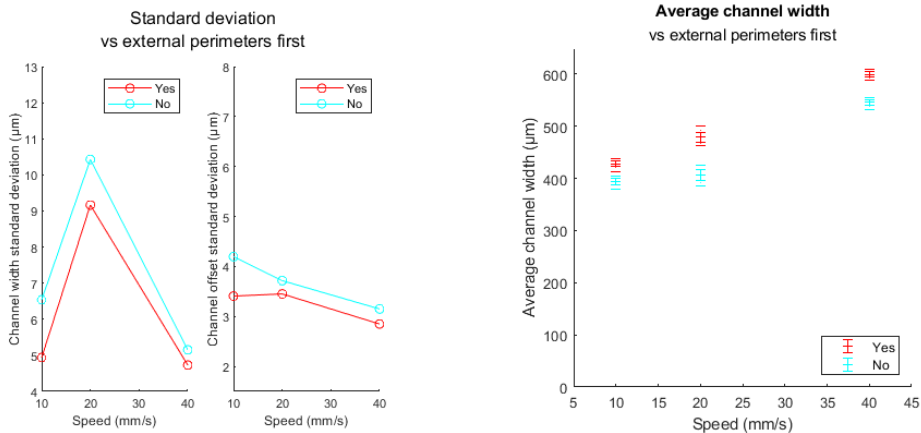
(a) Standard deviations of channel width and offset.

(b) Average channel width.

Figure 39: Graphs showing how different properties of the channel varied with movement speed and depending on if external perimeters were printed first (Yes) or not (No). a) shows how the standard deviation of the channel width and offset varied. b) shows how the average channel width varied, with error bars showing standard deviation and maximum positive and negative deviations.

Figure 39a seems to suggest that printing external perimeters first does slightly reduce the standard deviation of the channel width and offset. The effect is however not consistent in the maximum deviations, so it does not appear to completely overpower random variation.

Judging by figure 39b, printing external perimeters first also appears to make the channel slightly wider. This effect does seem to overpower random variation, since there is no overlap between the two options at any given speed even with maximum deviations.

4.7.2 Average distance between peaks and valleys and average pixel plateau length vs external perimeters first

(a) Distance between peaks and valleys on channel sides.

(b) Average pixel plateau length.
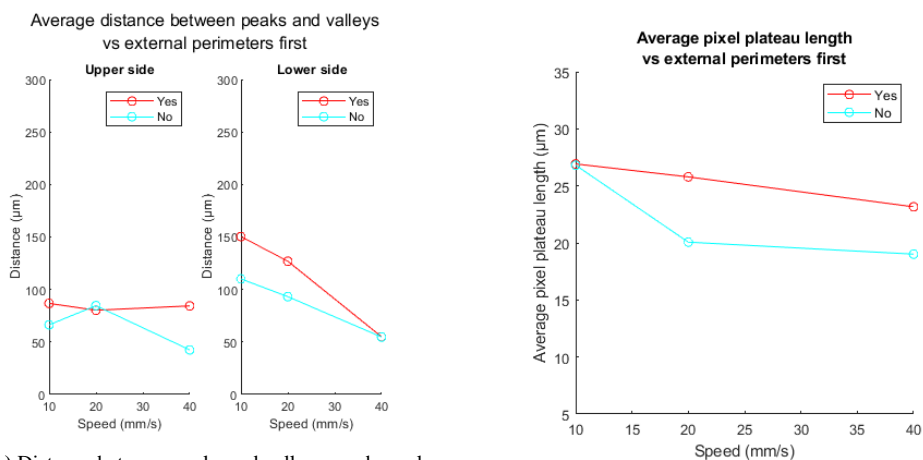
Figure 40: Graphs showing how different properties of the channel varied with movement speed and depending on if external perimeters were printed first (yes) or not (no). a) shows how the average distance between peaks and valleys in the shape of the channel sides varied, while b) shows how the average pixel plateau length varied.

That printing external perimeters first slightly improves quality is also supported by the average distance between peaks and valleys and average pixel plateau length. Figure 40 shows that, on average, the shape of the channel changes slightly more slowly if external perimeters are printed first.

Taken together, it appears that printing the external perimeters first quite consistently improves the quality of the channel somewhat, as it reduces the standard deviation of both channel width and offset and makes the the shape of the channel vary more slowly. The cause is likely that when external perimeters are not printed first, any unevenness present on the internal perimeters will influence the shape of the external perimeter. This would add any unevenness of the inner perimeters to the unevenness the external perimeter would have in isolation. This is also supported by that channels are slightly narrower when the internal perimeters are printed first, as they likely limit how the still liquid material of the external perimeter can spread out, causing it to be pushed more towards the center of the channel.

The effect of printing external perimeters first is not strong enough to change how FDM can be used on its own. It does however provide a simple and straightforward way to make a small but significant improvement to the quality of microfluidic devices made with FDM.

4.8 Nozzle diameter

Unlike all other parameters investigated in this paper, nozzle diameter is not a setting used to determine exactly how the 3D-printer will print an object, but rather a physical property

of the printer. The diameter of the original nozzle for this specific printer, or "base value" for this parameter, was 0.4 mm, a common nozzle size for FDM 3D-printers. To test different nozzle sizes, a separate set of nozzles with diameters of 0.2, 0.4, 0.6 and 0.8 mm, all from the same manufacturer, was used. As this set included a 0.4 mm nozzle, the original nozzle for the printer was not used to test this parameter, to avoid errors caused by significant variance in manufacturing methods.

Since the nozzle is what an FDM 3D-printer uses to "draw" objects, it directly limits the minimum size of positive features, such dividing walls between microfluidic channels (see figure 9). What the effects the nozzle size has on negative features, like the channels themselves, is less clear.

Unlike for the other parameters, to test nozzle sizes multiple samples (10 specifically) were made using the same settings. This also provided a sense for how much different measures could vary even while using the same settings. To process the data, the micrographs from the 10 samples were essentially placed after each other to form one very long channel, while compensating for the different samples having different average widths.

4.8.1 Channel width and offset deviation vs nozzle diameter

(a) Deviations of channel width.   **(b)** Deviations of channel offset.
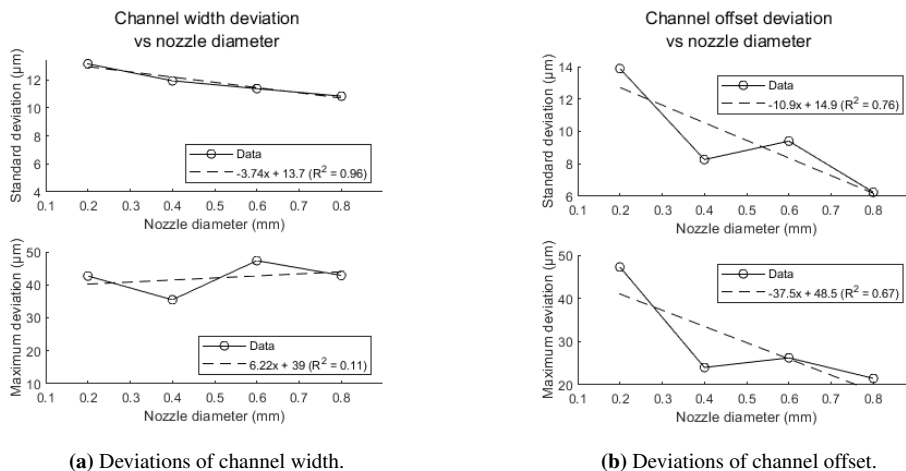
Figure 41: Graphs showing how the standard and maximum deviations of channel width and offset varied with nozzle diameter. a) shows the deviations of channel width while b) shows the deviations of channel offset. Note that in b) the y-axis ranges are not the same as in other graphs of these channel properties.

While figure 41a does seem to suggest that there is a correlation between nozzle diameter and the standard deviation of the channel width, the lack of such a correlation in the maximum deviation strongly suggests that it is a false positive. As can be seen in for example figures 35a to 35c, the standard and maximum deviations of channel width are usually closely related. Even if the correlation with standard deviation does exist as seen in figure 41a, it is not very useful; it is not feasible to use a nozzle larger than 1 mm, and it cannot be smaller than 0 mm, so the standard deviation would still be between 10 and 14 µm.

The correlation between nozzle diameter and channel offset deviations seen in figure 41b appears to be more likely to actually exist, since it is seen in both standard and maximum deviations. Such a correlation could feasibly be caused by there being less short distance random variation when using a larger nozzle, resulting in a more "averaged out" channel. This should however also have a similar effect for channel width, the existence of which is quite dubious.

The datapoint distribution seen in figure 41 is also quite similar to what is seen in figure 42a. This makes it quite possible that the correlation seen is between average channel width and deviations of channel offset, rather than between nozzle diameter and deviations of channel offset.

4.8.2 Average channel width and Fourier transform vs nozzle diameter

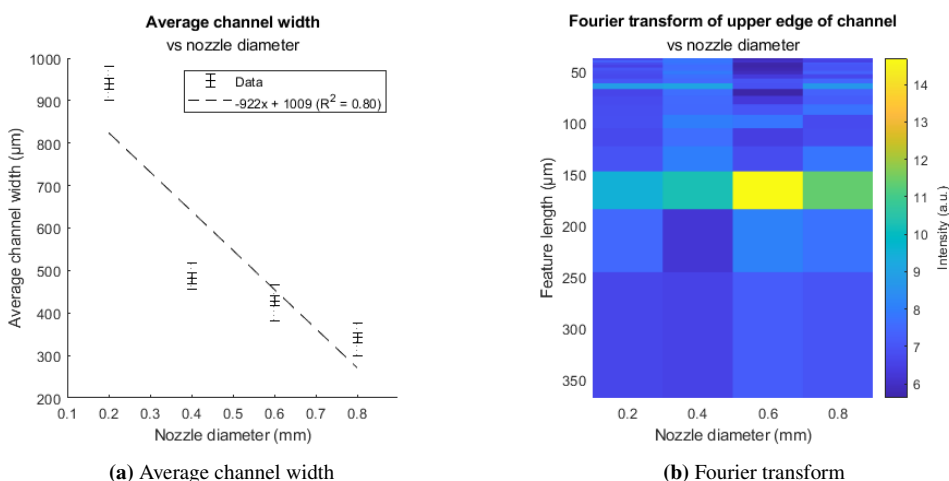(a) Average channel width   (b) Fourier transform

Figure 42: The graph in a) shows how average channel width varied with nozzle diameter, with error bars showing standard deviation and maximum positive and negative deviations. A linear fit has been added to enable easy comparison between different graphs. Note that the y-axis range is not the same as in other graphs of this channel property. The graph in b) shows the Fourier transform of the upper edge of the channels.

Figure 42a suggests that there is a pretty significant correlation between average channel width and nozzle diameter, especially considering that standard and maximum deviations can be taken into account. Considering that the 0.2 mm nozzle is a bit of an outlier, it does seem possible that the correlation is caused by increasing hydraulic resistance making it difficult for the extruder to push a sufficient amount of material through the nozzle.

This also lines up with observations made during the manufacturing of the samples. The supportive structure of the samples made with the 0.2 mm often were unusually frail and seemed to not be properly filled in with material, suggesting insufficient extrusion. It lines up with what is seen in the tests of both nozzle temperature and speed as well; the flow

rate through the nozzle is under normal circumstances somewhat limited by hydraulic resistance, and increasing this resistance reduces the amount of material that is deposited. This then results in thinner lines of material, which in turn leads to wider channels.

The intensity peak in the Fourier transform for features slightly smaller than 200 μm seen in figure 42b is odd. While it is close to what is seen in other Fourier transforms (an intensity peak slightly below 150 μm) it is distinctly different. There also does not seem to be any semblance of an intensity peak around 150 μm for the Fourier transforms of the nozzle diameter tests. This could possibly be due to the intensity for features slightly smaller than 200 μm only becoming clear when taking the average of a number of samples, while being mostly invisible when looking at individual samples, with the opposite being true for features slightly smaller than 150 μm. It could also simply be due to some error in the data processing.

4.8.3 Average pixel plateau length and channel width at end bumps vs nozzle diameter

(a) Average pixel plateau length.
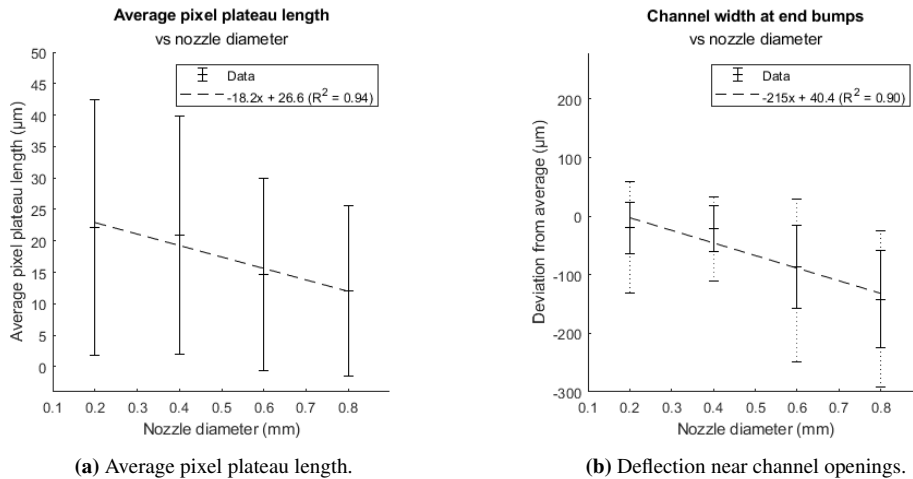
(b) Deflection near channel openings.

Figure 43: Graphs showing how average pixel plateau length and deflection at the ends of the channel varied with nozzle diameter, with error bars showing standard deviation. For b) error bars also show maximum positive and negative deviations. A linear fit has been added to enable easy comparison between different graphs. a) shows how the average pixel plateau length change varied with nozzle diameter. Note that the y-axis range is not the same as in other graphs of this channel property. b) shows how the change in width of the channel near the openings varied with nozzle diameter.

Looking at figure 43, both the average pixel plateau length and channel width at end bumps appear to be quite dominated by random variation. It is quite uncertain if nozzle diameter actually has correlations with average pixel plateau length and the width of the channel width at the end bumps, due to the very significant standard deviations. For average pixel plateau length even the smallest standard deviations are larger than the differences between averages. The correlation is also quite unexpected; scaling up the nozzle causes the channel shape to vary more rapidly, essentially "scaling it down" lengthwise.

The channel width at the end bumps does however have a more significant and more feasible correlation with nozzle diameter, especially if combined with the observations that the whole end bump structure seems to scale down with nozzle size, as seen in figure 44.

Previous tests of speed and acceleration suggests that the bumps are not caused by the extruder nozzle deviating from its intended path, instead being caused by a mismatch between movement speed and the rate at which material is deposited. It would then not be surprising if the size of these bumps is proportional to the amount of material being deposited. Since reducing nozzle size also reduces the width of the line used to "draw" layers, the amount of material being deposited should be directly proportional to nozzle size. This would be a very useful correlation, since it would mean that the issues caused by the end bumps, such as completely blocked channels, would shrink with nozzle size. The presence of this correlation in the data is however not certain, due to the significant standard and maximum deviations.


(a) Nozzle P2.   **(b)** Nozzle P4.   **(c)** Nozzle P6.   **(d)** Nozzle P8.

Figure 44: One end of the channel of samples made with different nozzle sizes. a) shows a channel made with nozzle P2, b) shows a channel made with nozzle P4, c) shows a channel made with nozzle P6 and d) shows a channel made with nozzle P8. Note that the "vertical channel" is an artifact of the data collection process rather than any form of side channel.

The lack of significant and impactful correlations between nozzle diameter and measures of channel quality is quite unexpected, since scaling down nozzle diameter and layer height essentially scales down the entire printing process. The tests of nozzle diameter did however only scale down the nozzle diameter; it might however be necessary to scale down both nozzle diameter and layer height to have the full effect.
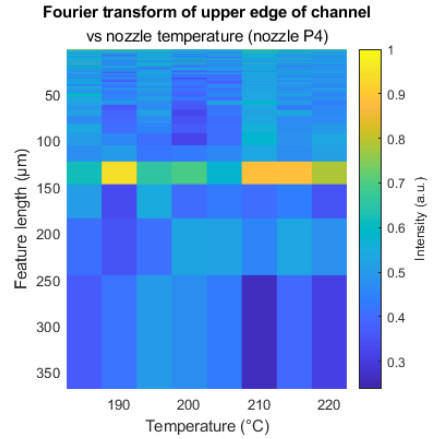
4.9 Fourier transforms

There does not seem to be any clear correlation between the Fourier transform of the upper edge of the channel and any of the tested parameters. As such those graphs have not been shown in the sections of the different parameters. There does however seem to be a tendency for there to be a higher than average intensity for a specific size of feature slightly smaller than 150 µm. To display this, the Fourier transforms have been given their own section. Figures 45 to 47 show some of the most clear examples of this.

Interestingly, this has not been noticeably affected by any parameter, including temperature, speed and layer height. This would suggest that the features likely depend on some form of spatial pattern on the 3D-printer, such imperfections in the wheels, bearings, tracks, belts, gears or stepper motors of the xy-stage, or the surface of the print bed. Features on the surface of the print bed seem especially likely; the surface is slightly rough to provide better adhesion to prints, and it is feasible that this roughness is on the scale of 150 µm.
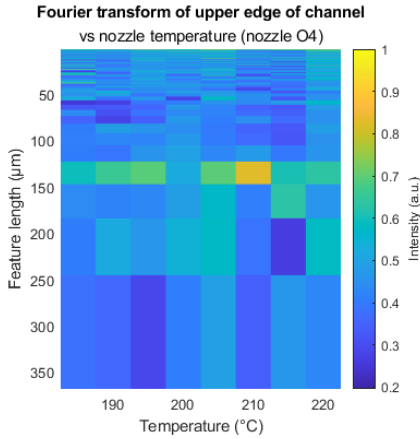
(a) Data from nozzle O4.

(b) Data from nozzle P4.

Figure 45: Graphs showing the Fourier transform of the upper side of the channel of the samples from the tests of temperature. The samples in a) were made using nozzle O4, while the samples in b) were made using nozzle P4.
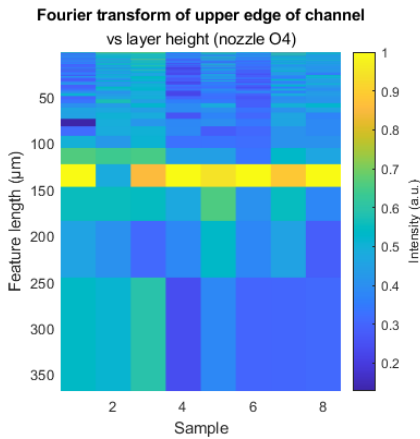
(a) Data from nozzle O4.

(b) Data from nozzle P4.

Figure 46: Graphs showing the Fourier transform of the upper side of the channel of the samples from the tests layer height. Since the layer height did not vary linearly, the x-axis is the sample number rather than the variable value. The samples in a) were made using nozzle O4, while the samples in b) were made using nozzle P4.
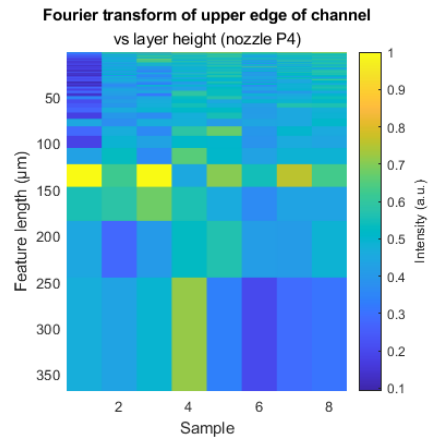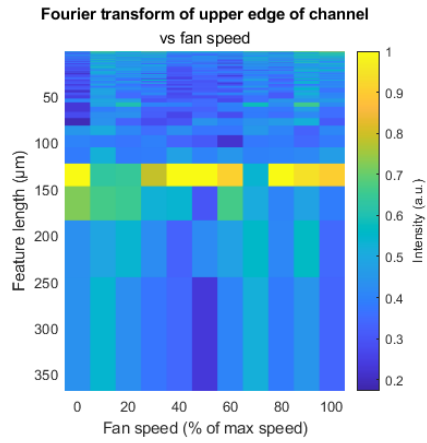
49

Figure 47: Graphs showing the Fourier transform of the upper side of the channel of the samples from the tests of cooling fan speed. The samples were made using nozzle O4.

5 General discussion

5.1 Consistent mechanisms

While most mechanisms discussed in section 4 are only supported by one or two measures done on one series of test, two mechanisms can explain results seen in tests of several different parameters.

5.1.1 The effect of hydraulic resistance on average channel width

Nozzle temperature (section 4.2.1), movement speed (section 4.3.1) and nozzle diameter (section 4.8.2) all seem to have an effect on the average channel width, in a way that would be consistent with that hydraulic resistance normally limits the rate at which the extruder deposits material.

Increasing movement speed, and through that extrusion rate, or decreasing nozzle temperature or diameter would all increase the hydraulic resistance in the extruder nozzle, which would hinder the deposition of material. Since the material still needs to fill the same amount of length, reducing the amount of material deposited would reduce the cross-section of the extruded line of material. Since the material still needs to go from the nozzle to the print bed if nothing else simply due to gravity, this reduction in cross-section would likely mainly influence the width of the line. Since, in the samples used in the tests, the center of the lines is always in the same position relative to the main channel, a reduction in the line width will lead to an increase in the channel width.

If consistent, such a variations in channel width are easy to compensate for by either changing the channel width in the 3D-model or adjusting settings in the slicer, if such exist. It could in fact even be useful, by potentially allowing more precise control of the channel width than the xy-stage of the printer would allow.

5.1.2 Over-extrusion caused by mismatch between movement speed and extrusion rate

Objects made with FDM never have perfectly sharp corners. While simply the round shape of the nozzle used to make them would prevent this, closer examination often shows not only roundness, but small bumps at the corners. This can easily be assumed to simply be due to the momentum of the extruder hotend causing it to "over-shoot" when changing direction at corners, especially since reducing the movement speed reduces the size of these bumps. Even closer examination, like then one done in this paper, does however show that such bumps are present on both sides of corners (here seen as being present on both the start and end of the one side of the test channels), whereas the bumps caused by momentum would only be present on one side.

Due to how speed (section 4.3.2) and acceleration (section 4.4.1) are related to the size of these bumps, a possible hypothesis is that they are caused by a mismatch between movement speed and extrusion rate. As the extruder hotend approaches a corner it slows down to prevent the previously mentioned bumps caused by acceleration. The extrusion rate meanwhile does not slow down, due to delays induced by the elasticity of the molten plastic and

the long section of filament between the feeder motor and hotend. This causes more material than intended to be deposited, which results in small "bumps" at corners made from the excess material.

This fits well with the data from the tests of movement speed. If it is assumed that the speed of the hotend at the point of the corner is always the same (likely controlled by the "xy-jerk" settings), the size of the bumps at the corner should be proportional to the extrusion rate. If the extrusion rate is assumed to be unchanged as the hotend decelerates and accelerates around the corner (a slight simplification), the extrusion rate should be proportional to the speed the hotend has before it starts decelerating, which is the movement speed. These taken together would mean that the size of the bumps should be proportional to movement speed, which is what is seen in the results.

How well this fits with the data from the tests of acceleration is a bit more difficult to analyse, due to the property of the data that is measured. The acceleration appears to affect how far the bumps extend before and after the corner. Specifically, it would appear that the factor that determines how much the over-extrusion causes the side to deviate from the intended shape is the speed in that specific point. This means that a reduced acceleration, which makes the speed change over a longer distance, causes the bumps to extend further.

The data this can be seen in however is the standard and maximum deviation of the channel width. The connection appears to be due to the residual deviation from the bumps affecting the channel width, causing it to gradually increase as their effect decreases (see figures 33 and 34). This makes it hard to determine the exact expected correlation between the parameter (acceleration) and measured property (channel width deviations). It should however at least be negative, which is what is seen in the data.

Since bumps like these would have a significant chance of blocking microfluidic channels, understanding them well would be quite important. Studies of the "xy-jerk" parameter, as well as further studies of speed and acceleration, would be useful for this purpose. A more detailed analysis of the shape of the corners would likely be useful in interpreting the data from such studies.

5.2   Error sources

Standard analysis of a dataset produced 9 different graphs showing different channel properties. This type of analysis was applied to 13 different datasets, resulting in over a hundred different graphs for there to be correlations in. As such it is very possible that there are a few false positives in the results of this paper.

Other than false positives, two major sources of error for the data in this paper have been identified: print bed calibration and print bed surface shape.

When making the samples used in this paper, the print bed was calibrated before each sample. This calibration was a quite manual procedure, being dependent on the operator being able to detect and remember minute differences in friction acting on a piece of paper. This resulted in there being some considerable variation in the exact calibration of the position and orientation of the print bed. Not calibrating was however not an option, since

the printing process seemed to slightly change the calibration without actually affecting the mechanisms (see figure 3) normally used to do so. While this change was smaller than the difference between manual calibrations, it had the potential to lead to drift over time, so manual calibration between prints was still used.

The printer used in this paper had a print bed surface that was removable and flexible, allowing easy removal of large prints and small prints. It was however found to not be completely flat, varying in height by more than 100 μm. It is believed, though not confirmed, that the combination of being removable and not completely flat strongly negatively influenced calibration, since there was no mechanism for ensuring that the print surface was placed back in exactly the same place after being removed. This could then result in that the relative heights at the calibration points and the area where the samples were printed could vary between prints.

The print bed surface was also slightly rough, to provide improved adhesion to prints. While this roughness has no negative effects on macroscopic prints, it is feasible that it affects small objects, like microfluidic channels printed directly on it, by causing the distance between the extruder nozzle and upper surface of the print bed to change as the nozzle moves.

5.2.1 Improvements to methodology

Most of the issues with calibration could possibly be avoided by checking the calibration of the print bed in the points where the microfluidic channels are to be printed, instead of over the calibration mechanisms. Using a printer that does not need to be calibrated between each print or is capable of automatic calibration would also make it easier to ensure that starting conditions are the same for every sample. While it is very much only a hypothesis, it is possible that the fact that the print bed moved during printing was what caused the changes in calibration on the printer used in this paper. Having a smooth and non-removable print surface, like the quite common glass surface, could also help alleviate the issues this paper had.

A different way to reduce issues with calibration would be to print the microfluidic channel on the second layer of a print, so that the walls of the channel do not directly touch the print bed. While this would make it more difficult to analyse the shape of the channel, it would prevent the channel from being affected by the print bed surface, and would provide a buffering layer that could reduce issues caused by variation in calibration. It is however possible that the shape of the channel would be affected by any unevenness caused by the printing process on the top surface of the first layer instead.

6 Conclusions

The micro-scale quality of channels made with FDM appear to be largely unaffected by the settings that determine how they are made, with the possible exception of layer height. While this does make it more difficult to improve this quality, it does provide a lot of freedom when attempting to improve other properties of the channels, such as structural integrity and transparency.

Interestingly, the size of the nozzle used to make the channels also appears to have little effect on the quality of the channels. While this does mean that making FDM suitable for making microfluidic devices is not as simple as making a tiny nozzle, it also means that it is not necessary to have a tiny nozzle to make microfluidic devices with FDM. The lack of correlation between nozzle size and channel quality also means that there are no negative consequences to using a small nozzle, which would otherwise limit the complexity and compactness of microfluidic devices made with FDM.

While the quality of individual channels is difficult to control, it is possible make channels where the width does not deviate by more than 15 μm, which is quite close to the optimal resolution of many FDM 3D-printers. This suggests that to make FDM useful for making microfluidic devices the focus does not need to be on improving optimal quality, but rather on improving quality consistency. Manufacturing truly microfluidic channels with FDM does however already seem very possible; even among the hundreds of chips made for this paper the channel width very rarely deviated by more than 30 μm.

Observations made during this project seem to suggest that using 3D-printers with automatic calibration and smooth print bed surfaces (like glass) could reduce issues with random variation when intending to make microfluidic devices with FDM.

An unexpected discovery was a possible mechanism for the omnidirectional "bumps" often seen on the corners of objects made with FDM. Judging by the data collected, they are likely caused by a mismatch between movement speed and material deposition rate. This is useful information, since such bumps could easily block microchannels if not compensated for. More research is however necessary to confirm that this hypothesis.

In summary, FDM can be used to make microfluidic channels in its current state, but more research is needed to achieve consistent quality and understand the sources of the various defects present.

References

[1] Eric K Sackmann, Anna L Fulton, and David J Beebe. The present and future role of microfluidics in biomedical research. *Nature*, 507(7491):181–189, 2014.

[2] Aniruddha M Kaushik, Kuangwen Hsieh, and Tza-Huei Wang. Droplet microfluidics for high-sensitivity and high-throughput detection and screening of disease biomarkers. *Wiley Interdisciplinary Reviews: Nanomedicine and Nanobiotechnology*, 10(6):e1522, 2018.

[3] Harold Craighead. Future lab-on-a-chip technologies for interrogating individual molecules. *Nanoscience and Technology: A Collection of Reviews from Nature Journals*, pages 330–336, 2010.

[4] George M Whitesides. The origins and the future of microfluidics. *Nature*, 442(7101):368–373, 2006.

[5] Claire E Stanley, Robert CR Wootton, and Andrew J deMello. Continuous and segmented flow microfluidics: Applications in high-throughput chemistry and biology. *CHIMIA International Journal for Chemistry*, 66(3):88–98, 2012.

[6] Michael J Beauchamp, Gregory P Nordin, and Adam T Woolley. Moving from millifluidic to truly microfluidic sub-100-μm cross-section 3d printed devices. *Analytical and bioanalytical chemistry*, 409(18):4311–4319, 2017.

[7] Benzion Amoyav, Yoel Goldstein, Eliana Steinberg, and Ofra Benny. 3d printed microfluidic devices for drug release assays. *Pharmaceutics*, 13(1):13, 2021.

[8] Charalampos Tzivelekis, Matthew P Selby, Albert Batet, Hojjat Madadi, and Kenny Dalgarno. Microfluidic chip fabrication and performance analysis of 3d printed material for use in microfluidic nucleic acid amplification applications. *Journal of Micromechanics and Microengineering*, 31(3):035005, 2021.

[9] Ken-ichi Ohno, Kaoru Tachikawa, and Andreas Manz. Microfluidics: applications for analytical purposes in chemistry and biochemistry. *Electrophoresis*, 29(22):4443–4453, 2008.

[10] Daniel Figeys and Devanand Pinto. Lab-on-a-chip: a revolution in biological and medical sciences., 2000.

[11] A. Folch. *Introduction to BioMEMS*. CRC Press, 2016.

[12] Amber L Boutiette, Cristoffer Toothaker, Bailey Corless, Chouaib Boukaftane, and Caitlin Howell. 3d printing direct to industrial roll-to-roll casting for fast prototyping of scalable microfluidic systems. *Plos one*, 15(12):e0244324, 2020.

[13] Muhammad Asif Ali Rehmani, Swapna A Jaywant, and Khalid Mahmood Arif. Study of microchannels fabricated using desktop fused deposition modeling systems. *Micromachines*, 12(1):14, 2021.

[14] Gregor Weisgrab, Aleksandr Ovsianikov, and Pedro F Costa. Functional 3d printing for microfluidic chips. *Advanced Materials Technologies*, 4(10):1900275, 2019.

[15] Reza Amin, Stephanie Knowlton, Alexander Hart, Bekir Yenilmez, Fariba Ghaderinezhad, Sara Katebifar, Michael Messina, Ali Khademhosseini, and Savas Tasoglu. 3d-printed microfluidic devices. *Biofabrication*, 8(2):022001, 2016.

[16] Anthony K Au, Wilson Huynh, Lisa F Horowitz, and Albert Folch. 3d-printed microfluidics. *Angewandte Chemie International Edition*, 55(12):3862–3881, 2016.

[17] Anna V Nielsen, Michael J Beauchamp, Gregory P Nordin, and Adam T Woolley. 3d printed microfluidics. *Annual Review of Analytical Chemistry*, 13:45–65, 2020.

[18] Niall P Macdonald, Joan M Cabot, Petr Smejkal, Rosanne M Guijt, Brett Paull, and Michael C Breadmore. Comparing microfluidic performance of three-dimensional (3d) printing platforms. *Analytical chemistry*, 89(7):3858–3866, 2017.

[19] Jia Min Lee, Meng Zhang, and Wai Yee Yeong. Characterization and evaluation of 3d printed microfluidic chip for cell processing. *Microfluidics and Nanofluidics*, 20(1):5, 2016.

[20] Andrew J Capel, Steve Edmondson, Steven DR Christie, Ruth D Goodridge, Richard J Bibb, and Matthew Thurstans. Design and additive manufacture for flow chemistry. *Lab on a Chip*, 13(23):4583–4590, 2013.

[21] Valentin Romanov, Raheel Samuel, Marzieh Chaharlang, Alexander R Jafek, Adam Frost, and Bruce K Gale. Fdm 3d printing of high-pressure, heat-resistant, transparent microfluidic devices. *Analytical chemistry*, 90(17):10450–10456, 2018.

[22] George M Whitesides, Emanuele Ostuni, Shuichi Takayama, Xingyu Jiang, and Donald E Ingber. Soft lithography in biology and biochemistry. *Annual review of biomedical engineering*, 3(1):335–373, 2001.

[23] Anthony K Au, Nirveek Bhattacharjee, Lisa F Horowitz, Tim C Chang, and Albert Folch. 3d-printed microfluidic automation. *Lab on a Chip*, 15(8):1934–1941, 2015.

[24] Hoang-Tuan Nguyen, Ha Thach, Emmanuel Roy, Khon Huynh, and Cecile Mong-Tu Perrault. Low-cost, accessible fabrication methods for microfluidics research in low-resource settings. *Micromachines*, 9(9):461, 2018.

[25] David J Beebe, Glennys A Mensing, and Glenn M Walker. Physics and applications of microfluidics in biology. *Annual review of biomedical engineering*, 4(1):261–286, 2002.

[26] Holger Becker and Claudia Gärtner. Polymer microfabrication methods for microfluidic analytical applications. *ELECTROPHORESIS: An International Journal*, 21(1):12–26, 2000.

[27] Holger Becker and Laurie E Locascio. Polymer microfluidic devices. *Talanta*, 56(2):267–287, 2002.

[28] Nirveek Bhattacharjee, Arturo Urrios, Shawn Kang, and Albert Folch. The upcoming 3d-printing revolution in microfluidics. *Lab on a Chip*, 16(10):1720–1742, 2016.

[29] Hua Gong, Bryce P Bickham, Adam T Woolley, and Gregory P Nordin. Custom 3d printer and resin for 18 μm$\times$ 20 μm microfluidic flow channels. *Lab on a Chip*, 17(17):2899–2909, 2017.

[30] Yang Liao, Jiangxin Song, En Li, Yong Luo, Yinglong Shen, Danping Chen, Ya Cheng, Zhizhan Xu, Koji Sugioka, and Katsumi Midorikawa. Rapid prototyping of three-dimensional microfluidic mixers in glass by femtosecond laser direct writing. *Lab on a Chip*, 12(4):746–749, 2012.

[31] Ho Nam Chan, Yiwei Shu, Bin Xiong, Yangfan Chen, Yin Chen, Qian Tian, Sean A Michael, Bo Shen, and Hongkai Wu. Simple, cost-effective 3d printed microfluidic components for disposable, point-of-care colorimetric analysis. *Acs Sensors*, 1(3):227–234, 2016.

[32] Lucas P Bressan, Cristina B Adamo, Reverson F Quero, Dosil P de Jesus, and José AF da Silva. A simple procedure to produce fdm-based 3d-printed microfluidic devices with an integrated pmma optical window. *Analytical methods*, 11(8):1014–1020, 2019.